Realistic Simulation of the *Aplysia* Siphon-Withdrawal Reflex Circuit: Roles of Circuit Elements in Producing Motor Output

J. R. LIEB, JR. AND W. N. FROST
Department of Neurobiology and Anatomy, University of Texas, Houston Health Science Center, Houston, Texas 77225

Lieb, J. R., Jr. and W. N. Frost. Realistic simulation of the *Aplysia* siphon-withdrawal reflex circuit: roles of circuit elements in producing motor output. *J. Neurophysiol.* 77: 1249–1268, 1997. The circuitry underlying the *Aplysia* siphon-elicited siphon-withdrawal reflex has been widely used to study the cellular substrates of simple forms of learning and memory. Nonetheless, the functional roles of the different neurons and synaptic connections modified with learning have yet to be firmly established. In this study we constructed a realistic computer simulation of the best-understood component of this network to better understand how the siphon-withdrawal circuit works. We used an integrate-and-fire scheme to simulate four neuron types (LFS, L29, L30, L34) and 10 synaptic connections. Each of these circuit components was individually constructed to match the mean or typical example of its biological counterpart on the basis of group measurements of each circuit element. Once each cell and synapse was modeled, its free parameters were fixed and not subject to further manipulation. The LFS motor neurons respond to sensory input with a brief phasic burst followed by a long-lasting period of tonic firing. We found that the assembled model network responded to sensory input in a qualitatively similar fashion, suggesting that many of the interneurons important for producing the LFS firing response have now been identified. By selectively removing different circuit elements, we determined the contribution of each to the LFS firing pattern. Our first finding was that the monosynaptic sensory neuron to motor neuron pathway contributed only to the initial brief burst of the LFS firing response, whereas the polysynaptic pathway determined the overall duration of LFS firing. By making more selective deletions, we found that the circuit elements responsible for transforming brief sensory neuron discharges into long-lasting LFS firing were the slow components of the L29-LFS fast/slow excitatory postsynaptic potentials. The inhibitory L30 neurons exerted a significant braking action on the flow of excitatory information through the circuit. Interestingly, L30 lost its ability to reduce the duration of LFS firing at high stimulus intensities. This was found to be due to the intrinsic nature of L30's current-frequency relationship. Some circuit elements, including interneuron L34, and the electrical coupling between L29 and L30 were found to have little impact when subtracted from the network. These results represent a detailed dissection of the functional roles of the different elements of the siphon-elicited siphon-withdrawal circuit in *Aplysia.* Because many vertebrate and invertebrate circuits perform similar tasks and contain similar information processing elements, aspects of these results may be of general significance for understanding the function of motor networks. In addition, because several sites in this network store learning-related information, these results are relevant for elucidating the functional significance of the distributed storage of learned information in *Aplysia.*

INTRODUCTION

Determining the exact functional roles played by different neurons and synaptic connections in neural circuits is not a simple matter. Even after detailed electrophysiological studies have worked out the basic structure of a particular circuit, the contribution made by each component to the processing of information as it flows through the network is often, at best, merely an educated guess. The *Aplysia* siphon-withdrawal reflex circuit is an interesting case in point. Although the basic form of the behavior is quite simple, the underlying circuitry is rather complex, consisting of monosynaptic and polysynaptic pathways, excitatory and inhibitory interneurons, chemical and electrical synapses, and a layer of interneuronal processing that includes both recurrent and lateral inhibition (Frost and Kandel 1995). What is the functional significance of all this complexity given the apparent simplicity of the behavior? Physiological studies have led to several speculations regarding the roles of the different components of this circuit (Cleary et al. 1995; Fischer and Carew 1993, 1995; Frost 1987; Frost and Kandel 1995; Hawkins and Schacher 1989; Hawkins et al. 1981; Trudeau and Castellucci 1992, 1993a,b; Wright et al. 1991), yet a means of testing these ideas has remained elusive.

One straightforward approach to determining the functional roles of the different circuit elements would be to study the effect on motor neuron firing of removing specific interneurons or pathways. Although this has been attempted in a few instances (Fischer and Carew 1993, 1995; Wright and Carew 1995), the fact that most interneurons in the circuit are multiply represented has made this approach rather difficult in practice. An alternative approach is to use physiological data to construct a realistic computer simulation of the circuit, which can then be used to study the detailed contribution of any neuron or synaptic connection to network function. Here we have used this latter approach to study the operation of the *Aplysia* siphon-elicited siphon-withdrawal reflex circuit. We employed a single-compartment, integrate-and-fire simulation scheme (Getting 1989a) to model all known circuitry conveying excitatory siphon-elicited input to one class of siphon motor neurons, the LFS cells. Our model network includes four neuron types (L29, L30, L34, and LFS), nine chemical synapses, and one electrical synapse (Fig. 1*A*).

In this paper we describe first the construction of our model, and then how the model was used to address several specific issues regarding the organization of the circuit. These issues include the following. What are the relative contributions of the monosynaptic and polysynaptic pathways to the characteristic phasic/tonic motor neuron firing response to sensory input? What specific role does interneuronal processing play in shaping motor neuron firing? For example, do each of the identified interneuron types (L29, L30, L34) make unique contributions to the motor neuron firing response, or are their contributions redundant? How do

0022-3077/97 $5.00

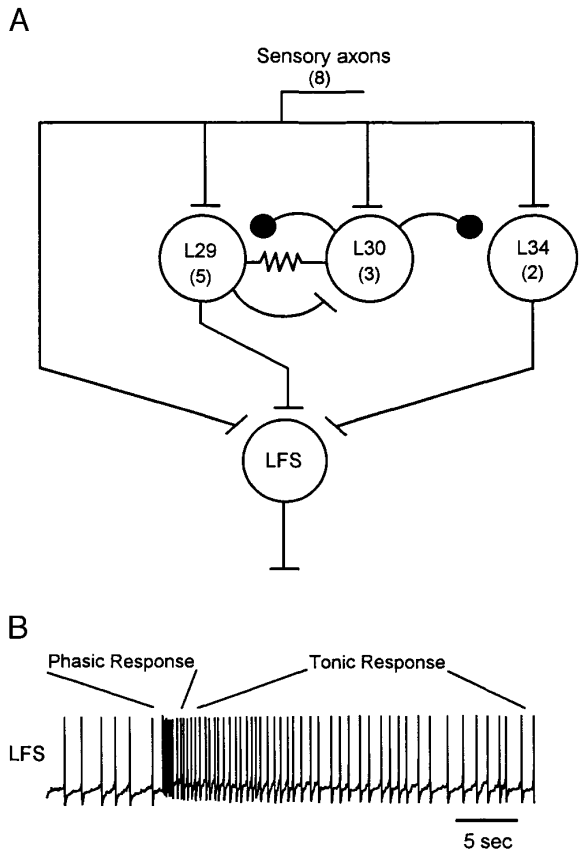

FIG. 1. *A*: circuit diagram of the modeled portion of the *Aplysia* siphon-elicited siphon-withdrawal reflex network. The model circuit represents 5 L29s, 2 L34s, 3 L30s, and an LFS siphon motor neuron. This circuit contains recurrent and lateral inhibition, electrical coupling, and both monosynaptic and polysynaptic sensory neuron to motor neuron pathways. *B*: physiological recording of an LFS siphon motor neuron response to a brief tactile siphon stimulus. These cells characteristically respond with a brief, high-frequency burst of action potentials (phasic response), followed by a long-lasting low-frequency spike train (tonic response).

the connections among the interneurons (electrical synapses, recurrent inhibition, and lateral inhibition) contribute to network function?

This study represents a detailed dissection of the functional roles of some of the different elements of the siphon-elicited siphon-withdrawal circuit in *Aplysia* (see also Blazis et al. 1993). These issues are of interest in part because this circuit has been used for some time as a model preparation for studies of learning-related cellular and synaptic plasticity (Byrne and Kandel 1996; Castellucci et al. 1970; Frost et al. 1988; Hawkins et al. 1993; Kandel and Schwartz 1982). In addition, because many features of the circuit, such as recurrent and lateral inhibition, are common to vertebrate motor circuits (Dowling 1992; Eccles 1964; Pompeiano 1984; Renshaw 1941), our results may have some relevance to motor circuits in general.

Some aspects of this work have been published previously in abstract form (Frost et al. 1991).

METHODS

Experimental preparation

A semi-intact preparation was used for all experiments, consisting of the abdominal ganglion attached by the siphon and branchial nerves to the gill, siphon, and other mantle organs. Animals (100–250 g) were anesthetized by injecting one third to one half their body weight of isotonic (350 mM) $MgCl_2$ into the hemocoel. After the ganglion and mantle organs were dissected out, the connective tissue surrounding the ganglion was lightly fixed by a 35-s exposure to 0.5% glutaraldehyde in artificial sea water (ASW) (Instant Ocean, Aquarium Systems). The entire preparation was next transferred to a two-chamber recording dish whose bottom surface was covered with a transparent Sylgard (Dow Corning) pinning surface. The abdominal ganglion was placed in the smaller of the two chambers, in a solution composed of 50% isotonic $MgCl_2$ and 50% ASW (maintained at 14–15°C), and the mantle organs were placed directly into ASW in the larger chamber (maintained at room temperature), with the siphon and branchial nerves passing through two narrow Vaseline-covered slits in a dividing wall between the two chambers. After the ganglion was pinned out and its left ventral side was desheathed, the CNS was revived by perfusing the smaller chamber with ASW. The siphon was revived by first injecting it directly with ASW, and then perfusing it throughout the experiment either through a polyethylene tube inserted into a sinus located in its base or through a needle inserted directly into its base. Both chambers were perfused separately throughout the experiment.

Cells were identified on the basis of their size, location, pigmentation, synaptic connections with other identified neurons, and response to tactile stimulation of the siphon (Frost and Kandel 1995; Hawkins et al. 1981). The LFS motor neurons were further identified on the basis of the characteristic siphon movements they produce when driven with intracellular current injection (Frost and Kandel 1995; Hickie and Walters 1995). Recordings were made with microelectrodes (10–20 MΩ) filled either with 3 M KCl or, when recording inhibitory postsynaptic potentials (IPSPs), with 4 M potassium acetate.

Modeling cells

Because our aim was to model the typical rather than an arbitrarily selected example of each neuron, we characterized the electrophysiological properties of each of the four cell types (L29, L30, L34, and LFS) in several different preparations. In each case, measurements were made of resting potential (V_r, the cell's membrane potential when at rest), input resistance (R_{input}, the asymptotic voltage change produced by a hyperpolarizing constant current pulse divided by the current applied), input capacitance (C, obtained by dividing the time constant of the input resistance charging curve by the input resistance itself), and steady-state action potential threshold (θ_{ss}, the membrane potential at which action potentials were initiated by just-threshold depolarizing constant current pulses). The spontaneously active LFS neurons were silenced by hyperpolarization before applying the depolarizing current pulses to determine θ_{ss}. The intracellular electrodes used in these recordings were carefully balanced before making measurements of R_{input} and θ_{ss}. All examples of each neuron type were from different preparations. After these measurements, all neurons were injected with a series of depolarizing constant current pulses to assess their repetitive firing properties (see RESULTS for details). Except for L29, all repetitive firing measurements were made in ASW. L29 posed the difficulty that it recruits recurrent IPSPs back onto itself from the L30 neurons, causing it to fire in a characteristic stuttering fashion (Frost et al. 1988). To eliminate this feedback and thus allow us to measure L29's intrinsic current-frequency relationship, we measured L29 excitability in three preparations in the presence of 100 μM *d*-tubocurarine, which blocks the L30 IPSP (Trudeau and Castellucci 1993a), thereby allowing L29 to fire smoothly to injected depolarizing current pulses.

Each model cell was constructed with the use of a four-step procedure (see APPENDIX for an explanation of the equations and parameters used in our simulation scheme). First, the experimen-

TABLE 1. *Mean measurements of cellular passive properties*

Cell	*n*	V_r, mV	R_{input}, MΩ	*C*, nF	θ_{ss}, mV
L29	8	−56.90 ± 2.16	14.7 ± 0.8	1.65 ± 0.31	−38.9 ± 3.5
L30	5	−48.40 ± 1.24	50.6 ± 4.5	1.00 ± 0.19	−37.8 ± 2.4
L34	5	−45.90 ± 3.26	35.3 ± 7.0	0.96 ± 0.21	−34.6 ± 2.7
LFS	9	−45.10 ± 1.71	65.6 ± 7.4	1.20 ± 0.13	−51.8 ± 2.3

Values, except *n* values, are means ± SE. V_r, resting potential; R_{input}, input resistance; *C*, input capacitance; θ_{ss}, steady-state action potential threshold.

tally measured mean values for V_r, R_{input}, and *C* were entered, which produced a model cell with passive properties very similar to those observed in soma recordings from its biological counterpart. Second, a threshold, defined by both a measured parameter (θ_{ss}) and two free parameters [threshold reset potential (θ_r) and time constant of decay of threshold θ_τ], and a fast spike undershoot conductance [reversal potential (E_{rev}) = −80 mV], defined by three free parameters [synaptic weight (*W*), opening time constant (τ_{open}), closing time constant (τ_{close})] were introduced. The five free parameters controlling threshold and the spike underhoot were then adjusted until the model cell's current-frequency plot for the first interspike interval matched that of the biological neuron for all but the highest current levels. To bring the firing rate at the highest current levels down to those observed experimentally, we next added one or two voltage-dependent shunt conductances (E_{rev} = V_r) to each model neuron and adjusted their free parameters [conductance (*G*), time constant of activation (τ_m), membrane potential at which steady-state activation was half-maximal (*B*), and slope parameter of the activation curve of the conductance (*C*)] to achieve the final match between the model and real first interspike interval curves. At this stage the model neurons would fire with an accurate initial instantaneous frequency, but showed no spike frequency adaptation. In the final step, two additional, slower undershoot conductances were added and their free parameters were adjusted to achieve a match of the current-frequency plot for the last interspike interval and the natural rate of adaptation within the firing train.

Modeling synapses

The procedure used to model each of the nine chemical synaptic connections in the circuit involved first simulating the waveform of the postsynaptic potential (PSP) and then setting its synaptic weight. PSP waveforms were recorded by placing intracellular electrodes in the pre- and postsynaptic neurons of each synapse and stimulating the presynaptic cell to fire either a single spike for fast PSPs, or a brief train of spikes for PSPs with slow components. PSP waveforms were recorded in a high-divalent cation solution [3 × Mg^{2+}, 3 × Ca^{2+}: 33 mM $CaCl_2$, 165 mM $MgCl_2$, 10 mM KCl, 390 mM NaCl, 10 mM tris(hydroxymethyl)aminomethane buffer] that raises neuronal thresholds in *Aplysia* (Byrne 1982; Byrne et al. 1978b), thereby decreasing polysynaptic recruitment and more cleanly exposing the monosynaptic connections of interest. Because we wanted to model the typical PSP waveform for each synapse in the network, we recorded several examples of each (1 per preparation) and chose a single representative example to model. The fast PSPs were observed to be quite similar for a given type of synapse. The slow PSPs, however, showed variability in duration from example to example. For modeling, we chose the median-duration slow PSP from all recorded examples of each connection type.

To model the waveform for each PSP, we drove the model presynaptic cell with the same firing pattern used to obtain the selected physiological example. For all fast PSPs, this was simply a single presynaptic action potential. For the slow PSPs made by L29 and L34, this involved duplicating the original presynaptic firing train. All PSPs were modeled with two or three parallel synaptic conductances, with the free parameters for each (*W*, τ_{open}, τ_{close}) adjusted until a close fit between the model and real PSP shapes was achieved. Synaptic E_{rev} was set at −60 mV for inhibitory connections and +10 mV for excitatory connections. These were not measured values, but were based on values obtained from other molluscan synapses (e.g., Getting 1989a).

After modeling the waveform of each synaptic potential, we next adjusted its weight (*W*). To do this, we adopted the procedure used by Getting (1983, 1989a), and adjusted *W* so that the presynaptic neuron would have the same effect on postsynaptic firing as observed in the real preparation in normal ASW. For all such connections, we collected synaptic strength data from several different preparations. We then rank ordered the data set for each connection with respect to effective strength (pre- vs. postfiring ratio for synapses made by interneurons, number of spikes in the phasic response to siphon touch for synapses made by sensory neurons) and chose the median strength example for modeling. The strength of each model synapse was set by replicating the stimulus conditions used during the experimental characterization of each synapse and then adjusting the weight terms (*W*) for the conductances underlying the synaptic connection until the model synapse displayed the same effective strength as the selected physiological example (see RESULTS for specific details). Because each chemical synaptic connection was composed of multiple independent conductances, the weight terms for all conductances composing a given PSP were scaled together by constant factors when adjusting synaptic strength to preserve PSP shape.

RESULTS

The portion of the siphon-withdrawal reflex circuit modeled in this study (Fig. 1) includes all presently known pathways that convey excitatory input from tactile siphon stimulation to the LFS motor neurons (Frost and Kandel 1995). Here we present *1*) our models of each cell and synaptic connection, *2*) a comparison of the real and model networks, and *3*) our use of the model network to determine the functional roles of the different circuit elements. See APPENDIX for a description of the equations used in our simulation scheme. The model network was constructed from data obtained from a total of 98 preparations.

Construction of the model

MODEL CELLS. We began by characterizing the resting properties of the different circuit neurons to obtain values for V_r, R_{input}, *C*, and θ_{ss} (Table 1). We found that the different cell types had different mixes of these features. For example, the L29 interneurons, which are silent at rest, had the deepest V_r and an 18-mV mean difference between their resting and steady-state threshold potentials. The LFS motor neurons, on the other hand, were active at rest, and thus had V_rs more positive than their steady-state threshold potentials.

The firing responses of each cell type to a wide range of injected currents are shown in Fig. 2. Figure 2*A* shows the

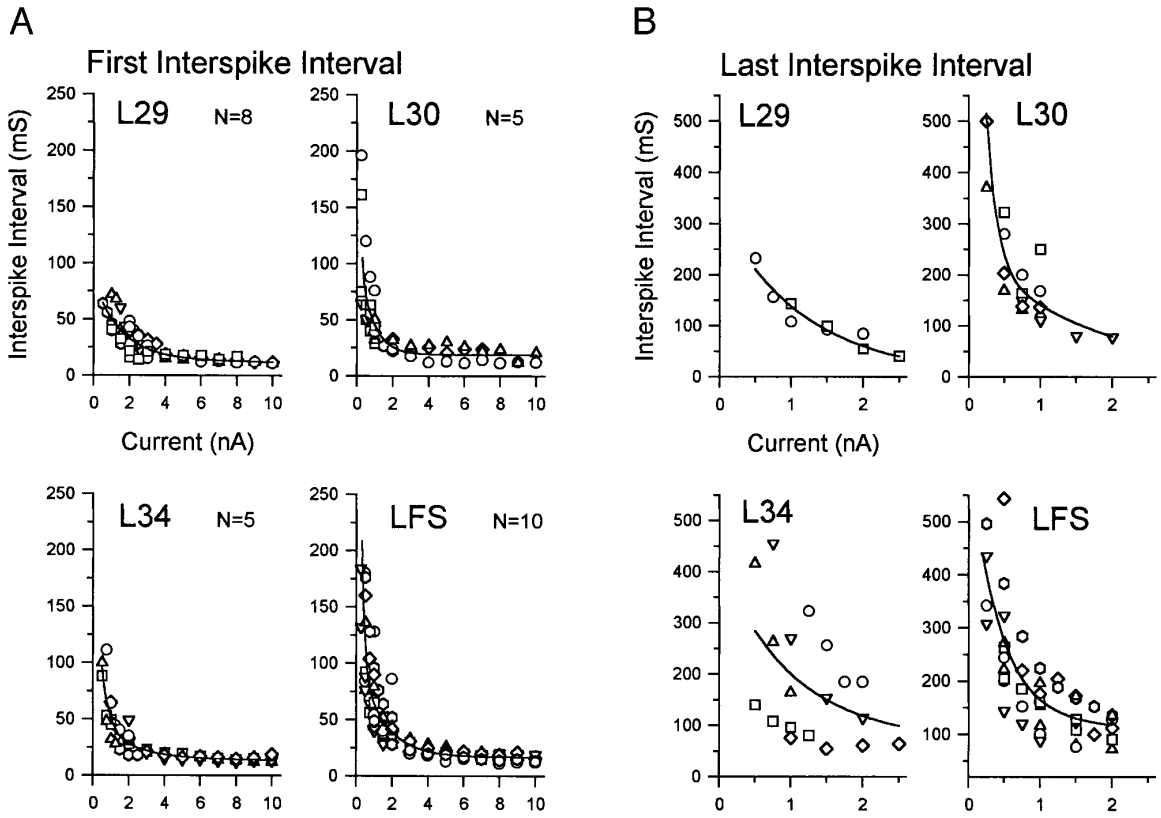

FIG. 2. Characterization of the repetitive firing properties of each of the biological neurons reconstructed in the model network. Cells were injected with a series of depolarizing constant current pulses (interpulse interval ≅ 2 min), and their firing responses were recorded. From 0 to 2.5 nA, pulses were 5 s in duration. Above 2.5 nA, pulses were shortened to 300 ms to avoid cell damage. The chosen upper current limit was 10 nA because such currents elicited firing responses that were as fast as or faster than the highest-frequency firing responses recorded in any circuit neuron to our standard 4-g punctate tactile siphon stimulus. Solid lines: double-exponential curve fits of the firing response data. Each neuron contributing to each data set is represented by a different symbol, and the total number of cells in each data set is indicated. All cells were from different preparations. *A*: plots of 1st interspike interval vs. current for all current pulses. *B*: plots of last interspike interval vs. current for 5-s current pulses only (0–2.5 nA). The last interspike interval data for L29 are from 3 preparations that were bathed in 100 μM *d*-tubocurarine, which was used to eliminate the recurrent inhibitory feedback from the L30s (see METHODS) and thereby expose L29's intrinsic degree of spike frequency adaptation. The curve fits from these plots, which represented the typical response profile of each cell type, were used as templates for constructing the model neurons (Figs. 3–6).

first interspike intervals for all firing responses. It can be seen that, although all cells had roughly similar initial firing rates at the highest currents, their responses to lower currents varied considerably. For example, although both L30 and LFS fired to the lowest levels of injected current, L29 had a higher threshold, and, once reached, L29 displayed a significantly higher initial firing rate than the other neurons. Figure 2*B* shows the last interspike interval for all firing responses to 5-s current pulses. The various cell types differed from one another with respect to this feature as well. For any given cell type, the difference between the first and last interspike interval curves represents the amount of spike frequency adaptation that developed in that cell type over the 5-s current pulse.

After plotting best-fit curves through the first and last interspike interval data for each cell type (Fig. 2), we then constructed model cells whose firing behavior matched these curves (see METHODS and figure legends for details). A comparison of the real and model L29 cells is shown in Fig. 3, including current-instantaneous frequency plots for a wide range (0–10 nA) of injected currents (Fig. 3*A*) as well as example firing responses and spike frequency adaptation profiles for two specific current pulses (Fig. 3, *B* and *C*). Comparisons of the real and model L30, L34, and LFS neurons are shown in Figs. 4–6, respectively. In all cases, we were able to construct integrate-and-fire model neurons that fired in very similar fashion to their biological counterparts over a wide range of injected currents.

MODEL PSP WAVEFORMS. Our next step was to model the PSP waveforms for each chemical synapse in the circuit. To do this, we conducted a series of electrophysiological experiments in which we impaled the pre- and postsynaptic neurons for each synapse and recorded the PSP waveform produced by activity in the presynaptic neuron. At all nine chemical connections, the presynaptic neuron produced fast excitatory postsynaptic potentials (EPSPs) or IPSPs onto the postsynaptic neuron (Fig. 7*A*). In addition, three of these connections (L29-L30, L29-LFS, L34-LFS) were dual component in nature, with a fast EPSP elicited by a single presynaptic action potential and an additional slow EPSP that persisted for several seconds following a train of action potentials (Fig. 7*B*). Our fits of all nine chemical PSP waveforms are shown in Fig. 7. The parameter values underlying all synaptic conductances are listed in Table 2. The numbers

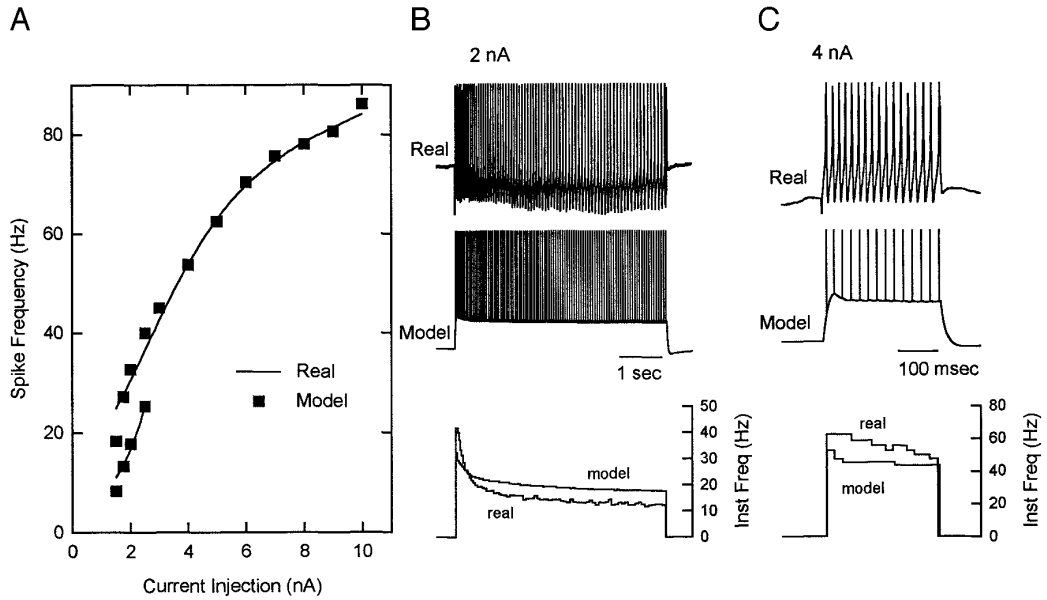

FIG. 3. Comparison of real and model L29 cells. *A*: instantaneous frequency-current plot of real and model neuron firing responses. In Figs. 3–6, the real responses, denoted by solid lines, are the best fit curves from Fig. 2 plotted as frequency. *Top data set*: instantaneous frequency of the 1st interspike interval for all firing responses. *Bottom data set*: instantaneous frequency of the last interspike interval for just the 5-s current pulses. The long pulses were used to characterize the spike frequency adaptation displayed by each cell type. *B*: firing responses of 1 physiological example, and the model L29, to a 5-s, 2-nA current pulse. The real L29 response was recorded in *d*-tubocurarine to eliminate recurrent inhibition from L30 (see METHODS). *B, bottom*: overlay of the 2 firing responses plotted as instantaneous frequency. *C*: firing responses to a 300-ms, 4-nA current pulse, with an overlay of instantaneous frequency shown below.

for R_{input} and V_r in Table 2 differ from the measured values in Table 1, because adding the electrical coupling between L29 and L30 shifted these properties in the simulation. The entered values for these parameters (Table 2) returned the model cell's R_{input} and V_r to their physiologically measured values.

MODEL SYNAPTIC STRENGTHS. The final step in constructing the model network was to adjust the strength of each synapse to mimic the median-strength example of its biological counterpart (see METHODS). These fits are shown in Figs. 8–10. Model synaptic strengths were set in the following order.

Interneuron connections. To measure the strength of the

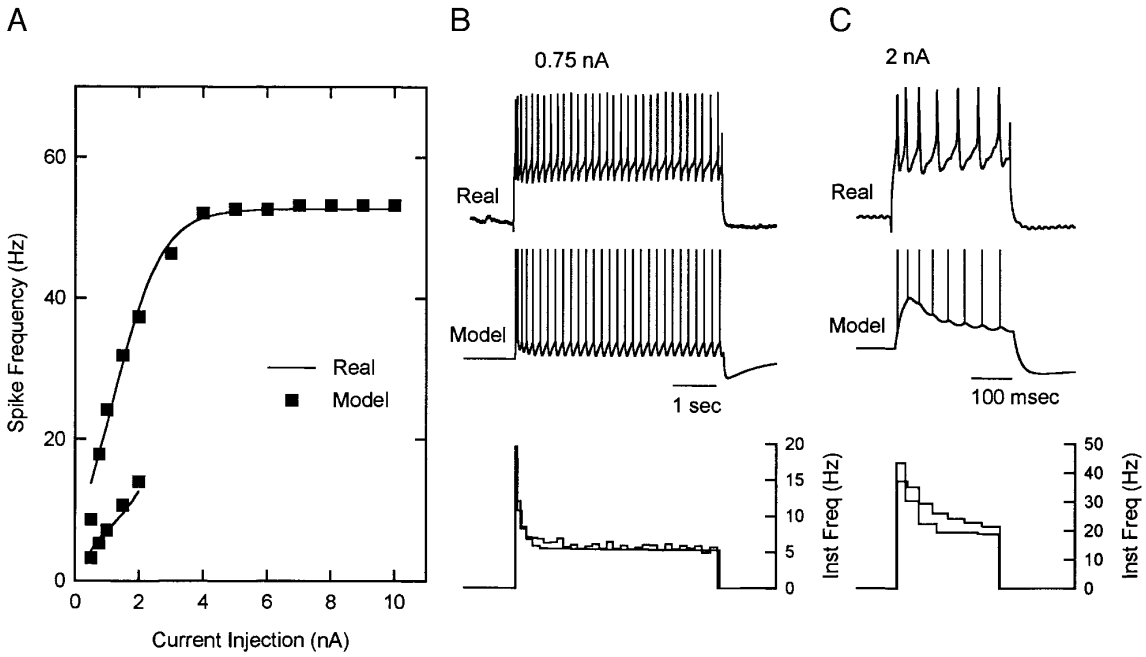

FIG. 4. Comparison of real and model L30 cells. *A*: instantaneous frequency-current plot of real and model neuron firing responses. Details as in Fig. 3. *B*: firing responses of real and model L30s to a 5-s, 0.75-nA current pulse. *C*: firing responses to a 300-ms, 2-nA current pulse.

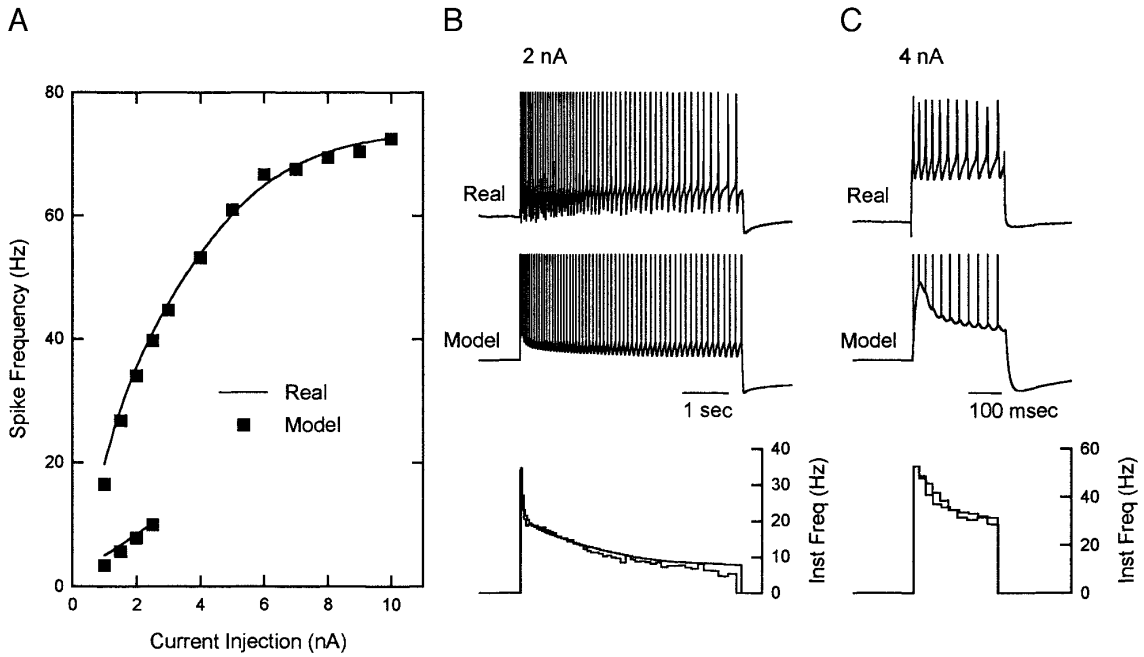

FIG. 5. Comparison of real and model L34 cells. *A*: instantaneous frequency-current plot of real and model neuron firing responses. Details as in Fig. 3. *B*: firing responses of real and model L34s to a 5-s, 2-nA current pulse. *C*: firing responses to a 300-ms, 4-nA current pulse.

electrical synapse between L29 and L30, the voltage deflection produced in each cell by the injection of a 1-s constant hyperpolarizing current pulse into the other cell was recorded. This connection was then modeled by introducing and adjusting a pair of unidirectional coupling resistances (R_{coupl}) between the model L29 and L30 neurons to duplicate the experimental data (not shown). The strengths of the L29-L30 and the L30-L29 chemical synaptic connections were evaluated by recording the ability of directly driven trains in each neuron to influence the firing of the other (Fig. 8, *A* and *B, top*). In the model network, the synaptic weights (W) of the L29-L30 and L30-L29 connections were then adjusted repeatedly until their experimentally recorded recurrent inhibitory interaction was reproduced as closely as possible (Fig. 8, *A* and *B, bottom*).

To measure the strength of the L30-L34 inhibitory connection, L34 was driven with constant current depolarizing pulses, both with and without L30 activation (Fig. 8*C, top*).

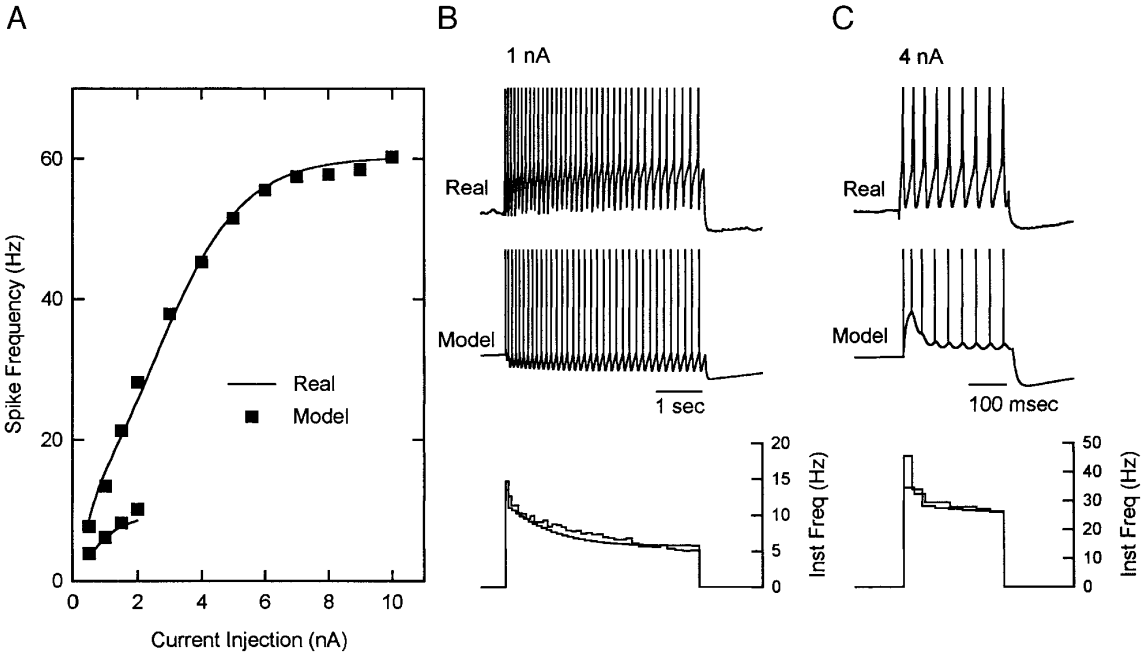

FIG. 6. Comparison of real and model LFS cells. *A*: instantaneous frequency-current plot of real and model neuron firing responses. Details as in Fig. 3. *B*: firing responses of real and model LFS neurons to a 5-s, 1-nA current pulse. *C*: firing responses to a 300-ms, 4 nA current pulse.

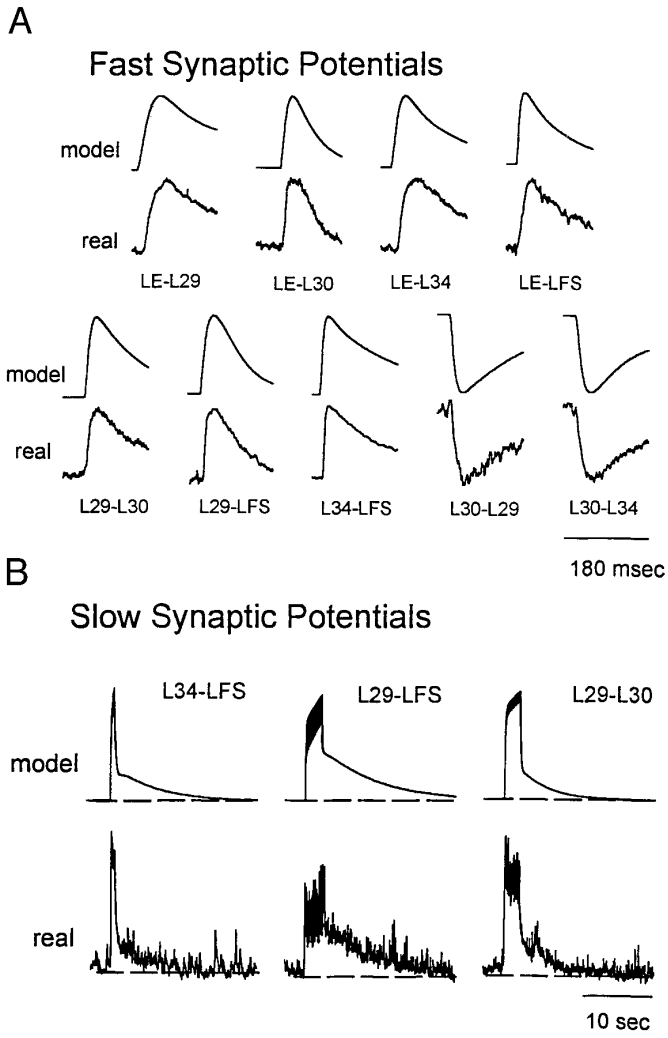

FIG. 7. Comparison of real and model postsynaptic potential (PSP) waveforms. The parameters used to construct these PSPs appear in Table 2. *A*: fast excitatory PSPs (EPSPs) and inhibitory PSPs (IPSPs). Each PSP was the result of a single action potential elicited in the presynaptic neuron. The physiological data set for each fast synaptic connection was: LE-L29, $n = 8$; LE-L30, $n = 2$; LE-L34, $n = 13$; LE-LFS, $n = 22$; L29-L30, $n = 4$; L29-LFS, $n = 23$; L34-LFS, $n = 30$; L30-L29, $n = 13$; L30-L34, $n = 7$. *B*: dual-component EPSPs. These were produced by driving the presynaptic neuron with the same action potential train as was used in the selected physiological example. The physiological data set for each slow synaptic connection was: L29-L30, $n = 6$; L29-LFS, $n = 25$; L34-LFS, $n = 29$.

This protocol was repeated with the model neurons and the weight of the L30-L34 synapse was adjusted to reproduce the experimentally recorded L30 inhibition of L34 (Fig. 8*C*, *bottom*).

To measure the strengths of the L29-LFS and L34-LFS interneuron to motor neuron connections, the effect of directly elicited activity in each interneuron on LFS firing was recorded experimentally (Fig. 9, *top*). This protocol was then reproduced with the model neurons, and their synaptic weights were adjusted to match the experimental data (Fig. 9, *bottom*).

Once the weight of each connection was set to match the median, experimentally recorded interaction between individual pairs of neurons, we scaled up the network to represent the total known numbers of each cell type. This was done by multiplying all synaptic weight terms by the number of known presynaptic neurons of that type in the preparation. Thus the *W* terms for all synaptic connections made by L29 were multiplied by 5, those made by L30 by 3, and those made by L34 by 2. This adjustment was made for the interneuronal synapses before the weights of the sensory neuron connections were set. Test simulations showed no difference in the shape, amplitude, or time course of synaptic potentials elicited by either five presynaptic cells firing one action potential simultaneously or by a single cell firing one action potential with its synaptic weight terms multiplied by 5.

Sensory neuron connections. The final step in network assembly was to set the weights of the sensory neuron connections (see METHODS). The procedure used for the interneuronal connections could not be applied to these connections, however, because the number of sensory neurons activated by our standard siphon stimulus is not known. Although previous work has estimated that a 4-g punctate siphon stimulus activates ~8 of the 24 LE sensory neurons (Byrne et al. 1978b), recent work has identified new siphon sensory neuron groups (Dubuc and Castellucci 1991), including one low-threshold group that contributes to LFS input, but whose cell bodies are not yet located (Cohen et al. 1991; Fischer and Carew 1993; Kaplan et al. 1993). To address this uncertainty, after all interneuronal synaptic weights had been set we adjusted the weights of the model sensory synapses to yield firing responses in the model neurons that matched, with respect to the number of spikes in their phasic bursts, the median experimental response of each neuron type to the standard siphon stimulus (Fig. 10). The standard stimulus consisted of a brief (~250 ms) press of the siphon against the chamber bottom with a hand-held nylon bristle calibrated to deliver a 4-g force (measured on a laboratory balance) when pushed to its bending point. Because the duration of the siphon stimulus was under subjective control, it should be considered to be a rough approximation to 250 ms.

In the model network, sensory neuron activity was mimicked by activating 32 total spikes in eight sensory axons (4 spikes per axon, see Fig. 12*A*). The pattern of discharge was arranged so that it rose rapidly to a peak frequency response at 25–50 ms after stimulus onset, and then rapidly declined to a constant, much lower firing frequency that terminated 230 ms after stimulus onset (see Fig. 12*A*). This discharge pattern was based on reported responses of LE sensory neurons to 4-g punctate siphon stimuli (Byrne et al. 1974, 1978a,b).

In setting the synaptic weights of the sensory neuron synapses, the sensory neuron connections onto L29 and L30 were set first, followed by the sensory neuron to L34 connection. This order ensured that we obtained the proper activation of L34, incorporating both its excitation by the sensory neurons and its inhibition by the L30s. The weight of the model monosynaptic sensory neuron to LFS synapse was set last, after all other circuit connection weights had been fixed. The median maximum instantaneous frequency of the responses of 11 real LFS neurons to the standard stimulus was 42.8 Hz. The maximum instantaneous frequency of the model LFS response was 40.0 Hz.

Evaluation of the model network

COMPARISON OF REAL AND MODEL NETWORKS. Once the cells, synaptic waveforms, and synaptic weights were set,

TABLE 2. *Parameters describing the model network*

Neuron	R_{input}, mΩ	C, nF	V_r, mV	θ_{ss}, mV	θ_r, mV	θ_τ, ms
			A. Cell parameters			
L29	15.7	1.65	−57.57	−38.9	75	9.0
L30	57.5	1.00	−47.06	−37.8	200	11.5
L34	35.3	0.96	−45.90	−34.6	200	10.0
LFS	65.6	1.20	−45.10	−51.8	200	10.0
	G		E_{Rev}, mV	*B*		*C*
			B. Voltage-dependent shunt conductances			
L29 shunt						
1	0.05		−56.9	30		−2
2	0.28		−56.9	13		−1
L30 shunt						
1	1.00		−48.4	−11		−1
L34 shunt						
1	0.09		−45.9	−20		−2
2	0.01		−45.9	−15		−1
LFS shunt						
1	0.10		−45.1	13		−2
2	0.18		−45.1	5		−2
Synapse	*W*		E_{Rev}, mV	τ_{open}, ms		τ_{close}, ms
			C. Spike undershoot conductances			
L29						
IK1	0.0375		−80	10		25
IK2	0.0030		−80	100		250
IK3	0.0004		−80	750		2,000
L30						
IK1	0.0600		−80	10		50
IK2	0.0125		−80	100		500
IK3	0.0005		−80	250		2,000
L34						
IK1	0.0750		−80	10		25
IK2	0.0250		−80	25		175
IK3	0.0035		−80	500		4,000
LFS						
IK1	0.2500		−80	10		50
IK2	0.0100		−80	40		750
IK3	0.0040		−80	750		2,000
			D. Interneuronal synaptic conductances			
L29-L30						
1	0.0396		10	6		11
2	0.0029		10	50		75
3	0.0004		10	100		3,500
L30-L29						
1	0.0328		−60	5		10
2	0.0281		−60	10		120
3	0.0038		−60	200		1,000
L30-L34						
1	0.0850		−60	6		15
2	0.0400		−60	15		200
3	0.0050		−60	200		1,000
L34-LFS						
1	0.0031		10	5		25
2	0.0001		10	50		275
3	0.0003		10	500		4,000
L29-LFS						
1	0.0255		10	5		9
2	0.0011		10	600		6,500

TABLE 2. *(continued) Parameters describing the model network*

Synapse	W	E_{Rev}, mV	τ_{open}, ms	τ_{close}, ms
		E. Sensory neuron synaptic conductances		
LE-L29				
1	0.0183	10	10	25
2	0.0208	10	15	300
LE-L30				
1	0.0600	10	2	9
2	0.0200	10	5	10
LE-L34				
1	0.2228	10	5	30
2	0.0331	10	75	100
LE-LFS				
1	0.0339	10	12	25
2	0.0033	10	50	170

Synapse	Coupling Resistance, MΩ
F. Electrical coupling between interneurons	
L29-L30	203
L30-L29	357

θ_r, threshold reset potential; G, conductance; E_{rev}, reversal potential; B, membrane potential at which steady-state activation was half-maximal; C, slope parameter of activation curve of conductance; W, synaptic weight; τ_{open}, opening time constant; τ_{close}, closing time constant; θ_τ, threshold decay time constant; for other abbreviations, see Table 1.

all parameters were fixed and the model was ready to be tested. Table 2 contains all parameter values for the finished model siphon-withdrawal network. Figure 11 compares the activity of the real and model networks to activation produced by the standard input stimulus. As can be seen, the model neurons fired quite similarly to their real counterparts.

What does this similarity between real and model circuits tell us about how close we may be to identifying the important circuit elements for the LFS component of the reflex network? During network construction, the weights of the sensory neuron connections onto the different circuit elements were deliberately set so that the model phasic firing responses matched the real responses. This was done both because we do not know how many sensory neurons are activated by siphon stimulation, and also because it was necessary to have realistic interneuronal firing responses before evaluating their respective roles in network function.

Although this method leaves us unable to comment on the degree to which the sensory population for this response has been identified, we can draw some conclusions about the nature of the sensory input. For example, although the intensities of the interneuron bursts were deliberately set when adjusting sensory axon synaptic weights, the durations of the bursts were an emergent property of the network, based on our realistic reconstructions of the individual waveforms of each PSP in the circuit. This suggests that, if additional, non-LE sensory neurons are contributing to these phasic responses, they must be producing fast PSPs of similar duration to the LE EPSPs used in the model. If their PSPs were significantly longer in duration, we would expect to observe significant differences between real and model burst durations.

In contrast, the model tonic LFS response was entirely an emergent property of the model, resulting from the neurons and synaptic connections so far identified in the network. The qualitatively similar response profiles of the real and model tonic LFS firing responses suggests that many of the essential circuit elements contributing to this LFS response component have now been identified.

ROBUSTNESS OF THE MODEL NETWORK. One concern with any simulation is the degree to which the chosen parameter set yields a cell or network that behaves in a stable, satisfactory fashion over a wide range of input conditions. We tested the robustness of the model network to a range of input strengths by varying the synaptic weight (W) of all sensory connections in the network in tandem from 0.25 to 4 times their control values and observing the LFS firing responses (Fig. 12). The smoothly graded phasic/tonic firing response of the model LFS neuron across this input range indicates that the model network is robust over a wide range of input intensities. Nearly identical LFS firing responses were obtained when input strength was varied by changing sensory axon stimulation frequency from 0.25 to 4 times control values as an alternative to changing synaptic weights. In physiological experiments, we found that a similar range of punctate siphon stimuli (1, 4, and 14 gm) each elicited this same phasic/tonic form of LFS firing response (not shown).

Use of the simulation to determine the roles of the various circuit components in network function

Once we had completed and tested the model network, we next turned to the main goal of the study: determining the roles of the different circuit elements in producing the characteristic LFS firing response profile to sensory input. To do this, we systematically deleted individual components of the circuit and examined their effect on LFS firing.

REMOVAL OF THE MONOSYNAPTIC VS. POLYSYNAPTIC PATHWAYS. In this study, ''monosynaptic'' pathway refers to the fast excitatory input to LFS that is exclusive of the known excitatory interneuronal inputs. The monosynaptic pathway thus includes direct input to LFS from the well-characterized

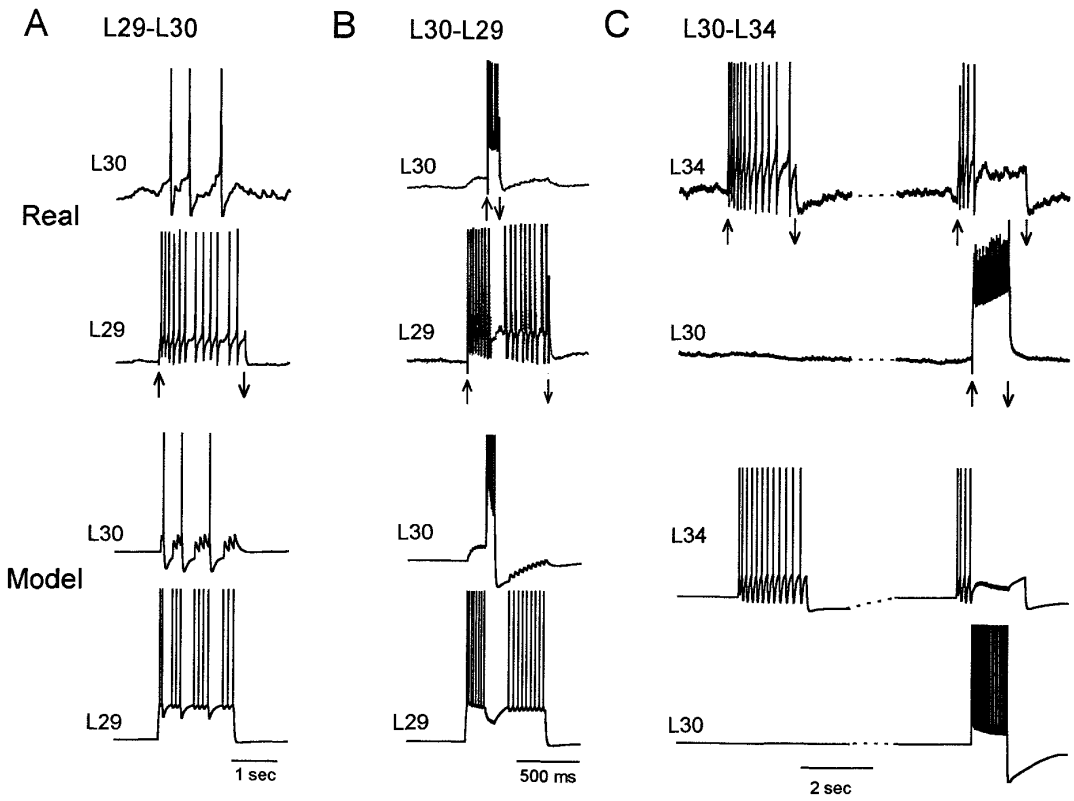

FIG. 8. Comparison of real and model interneuron to interneuron connection strengths. Each model synapse was adjusted to have the same functional connection strength (the same effect of presynaptic activity on postsynaptic firing) as its biological counterpart (see METHODS). In each case, the *top pair of traces* depicts the physiological recording selected to model; the *bottom pair of traces* shows the connection strength of the corresponding synapse in the model network. *A*: L29-L30 excitatory synapse ($n = 7$). A depolarizing constant current pulse (↑ ↓) was used to elicit a train of action potentials in L29, and the firing response in L30 was recorded. *B*: L30-L29 inhibitory synapse ($n = 7$). L30 was held hyperpolarized, and then was depolarized briefly (↑ ↓) to produce inhibition of an elicited L29 train (↑ ↓). *C*: L30-L34 inhibitory synapse ($n = 1$). *C, left*: depolarizing current pulse (↑ ↓) elicited firing in L34. *C, right*: L30 was depolarized to fire (↑ ↓) during a 2nd depolarizing current pulse in L34 (↑ ↓), which inhibited L34's response.

LE sensory neurons as well as any other sensory neuron groups activated by siphon stimulation that excite the LFS neurons. Because the weight of the monosynaptic connection was based on the responses of LFS neurons to siphon stimuli, it is also possible that it includes as yet unidentified excitatory interneurons in the sensory neuron to LFS motor neuron pathway. All LFS firing responses were analyzed with respect to four measures: the maximum frequency and duration of the phasic firing response component, and the maximum frequency and duration of the tonic firing component (Fig. 13*A*).

One of our first findings with the model network was that the monosynaptic and polysynaptic pathways mediate separate aspects of the LFS firing response. Of the two components, phasic and tonic, of this response (Fig. 13*A*), removal of the monosynaptic pathway (Fig. 13*B1*) affected only the phasic component. This involved a substantial drop in the maximal frequency of the phasic burst at all stimulus intensities, and a reduced burst duration at weak stimulus intensities (Fig. 13*B2*). The tonic firing component was essentially unaffected (Fig. 13*B3*).

On the other hand, removal of the polysynaptic pathway (Fig. 13*C1*) had just the opposite effect. This included no effect on the maximum frequency of the phasic LFS firing component (Fig. 13*C2*), a decrease in the duration of the phasic component at moderate to strong stimulus intensities (Fig. 13*C2*), and a total elimination of the tonic firing response (Fig. 13*C3*).

To explicitly test the contributions made by fast versus slow PSPs in the network, we compared the results of three simulations (Fig. 14): a control simulation, a simulation in which the slow synaptic components of the interneuron to motor neuron connections were removed from the network, and a simulation in which all fast EPSP connections onto LFS were removed. When only fast connections were present, the LFS neuron had a phasic but no tonic firing component. When only slow connections were present, LFS had a tonic but no phasic firing component. These results make it clear that the slow components of the interneuron to motor neuron synapses are entirely sufficient to mediate the transformation of brief sensory neuron discharges into the characteristic long-lasting LFS firing response.

REMOVAL OF THE DIFFERENT CIRCUIT INTERNEURONS. We next tested the role of each interneuron type in network function (Fig. 15). Of all the interneurons, L29 was found to have the largest influence on motor neuron firing (Fig. 15*A1*). Removing L29 produced no change in the maximal frequency of the phasic LFS firing component (Fig. 15*A2*), a reduced duration of the phasic component at high stimulus intensities, and an elimination of the tonic firing response (Fig. 15*A3*). This latter result indicates that, of the two types of excitatory interneurons, the slow EPSP made by the L29s onto LFS is the key circuit

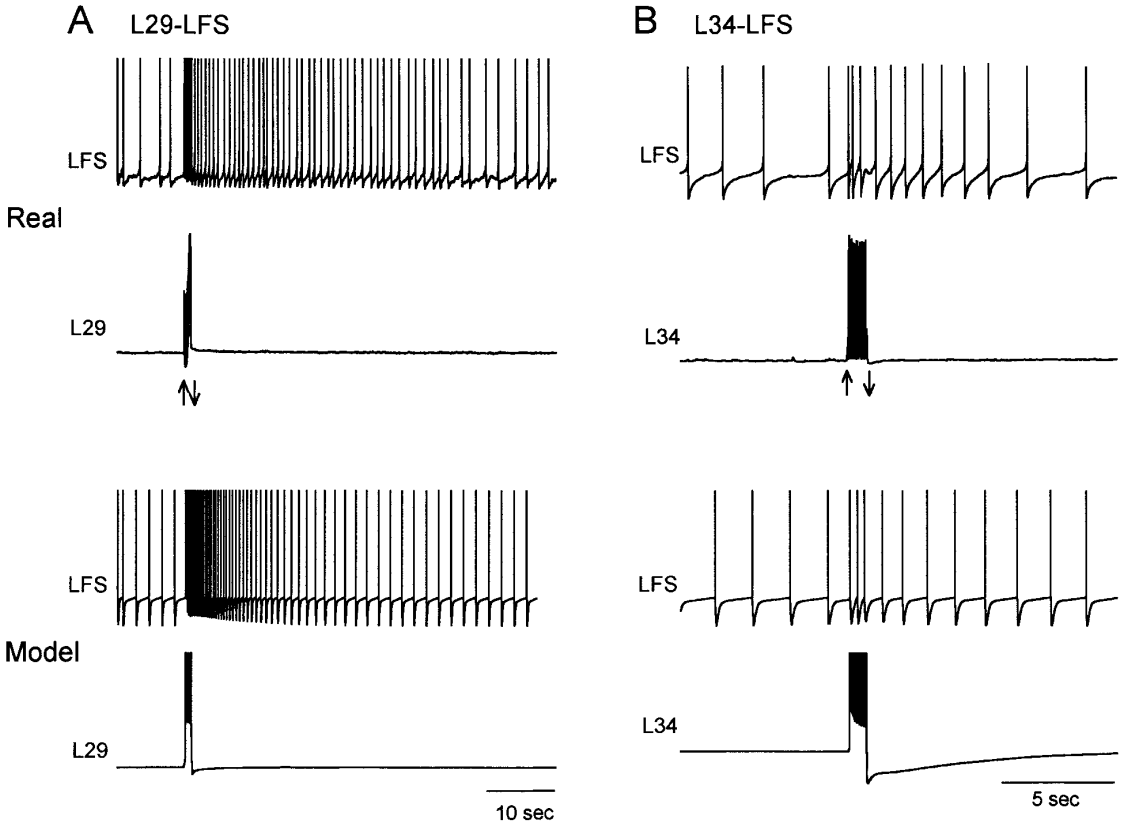

FIG. 9. Comparison of real and model interneuron to motor neuron connection strengths. Depolarizing constant current pulses were applied to L29 and L34 (↑↓) and the firing response of LFS was recorded. In each case, the *top pair of traces* depicts the physiological recording selected as the median strength example from all recordings of that synapse, and the *bottom pair of traces* shows the connection strength of the corresponding synapse in the model network. *A*: L29-LFS synapse ($n = 4$). *B*: L34-LFS synapse ($n = 11$).

locus for transforming brief sensory discharges into long-lasting motor neuron firing.

Deleting L30 (Fig. 15*B1*) revealed an important braking role for this neuron in normal network function. As for L29, L30 deletions affected the duration of the phasic LFS burst (Fig. 15*B2*) as well as both components of the tonic firing response (Fig. 15*B3*). These effects were in the opposite direction to those obtained with L29 deletion, however, consistent with L30's inhibitory role in the circuit.

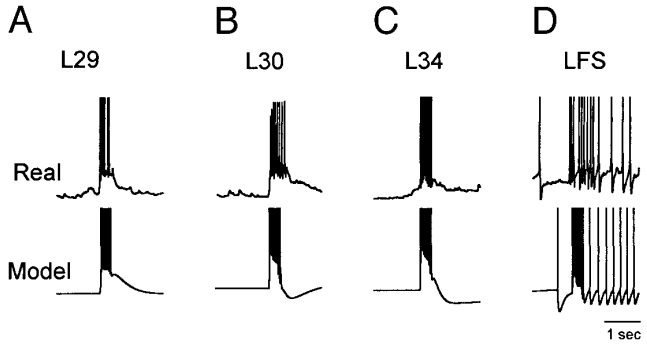

FIG. 10. Comparison of real and model neuron responses to sensory input. *Top traces*: median-strength response of each circuit neuron type to a 4-g, ~250-ms punctate siphon stimulus. *A*: response of L29 ($n = 10$). *B*: response of L30 ($n = 6$). *C*: response of L34 ($n = 12$). *D*: response of LFS ($n = 11$). *Bottom traces*: response of each model neuron to the sensory axon discharge pattern (see Fig. 12*A*) used to deliver sensory input to the model network.

One unanticipated result that initially surprised us was that L30 deletion elevated the duration of the tonic LFS firing response at low but not high stimulus intensities. While considering the possible cause of this effect, we noted that L30's current-frequency plot tended toward an asymptote at high current levels, such that above a certain point, injection of stronger currents failed to significantly increase L30's firing rate (Fig. 4*A*). To test the possibility that this intrinsic property of L30 was responsible for its inability to inhibit the duration of the LFS tonic firing response at high stimulus intensities (Fig. 16*A*), we constructed an alternate L30 that had a continually rising current-frequency plot, similar to those of the other circuit neurons (Fig. 16*B*). An assessment of circuit performance with the two different L30s revealed that the asymptotic shape of the L30 current-frequency relationship was the circuit feature responsible for the loss of L30 effectiveness at high stimulus intensities (Fig. 16*C*).

L34 deletion had virtually no effect on any component of LFS firing (Fig. 15*C*). This is presumably due to the smaller number of L34s than L29s (2 vs. 5) and the significantly weaker weight of the L34-LFS connection compared with the L29-LFS connection (see Fig. 9 and Table 2). Taken together, these interneuronal deletions indicate that the different cell types vary greatly in both their quantitative and qualitative contributions to network function, particularly when examined across a range of stimulus intensities. They also demonstrate that intrinsic cellular properties can be just

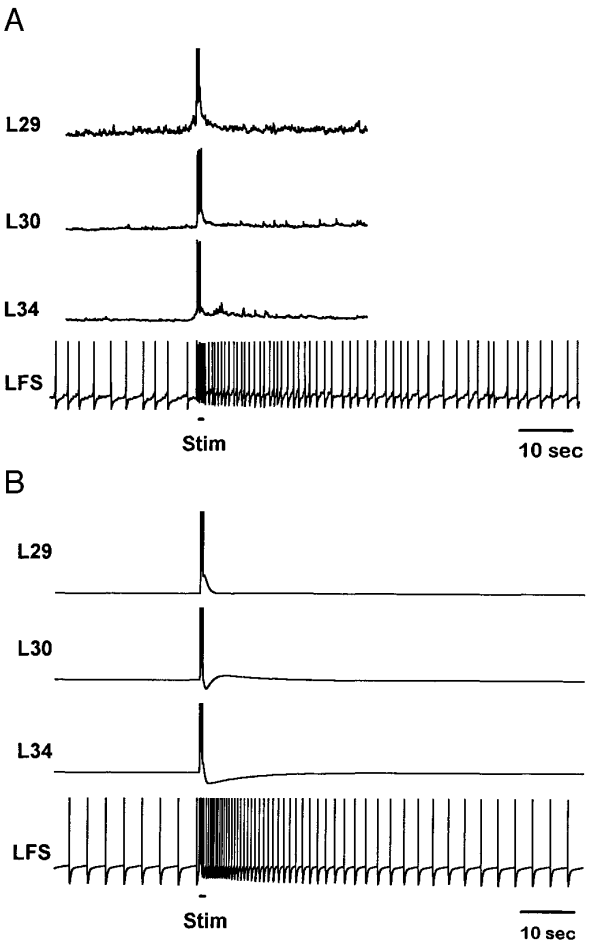

FIG. 11. Comparison of the real and model networks. *A*: response of the real circuit to a 4-g, ~250-ms punctate siphon stimulus. Traces are from different preparations. *B*: response of the model network to the sensory axon discharge pattern used throughout the study (see Fig. 12*A*).

as important as synaptic properties in determining network responses to sensory input.

REMOVAL OF DIFFERENT CATEGORIES OF INTERNEURONAL CONNECTIONS. After characterizing the role of each circuit neuron, we examined the roles of the different classes of synaptic connections in the circuit (data not shown). These included recurrent inhibition, lateral inhibition, and electrical coupling. Removing recurrent inhibition by taking out the L30-L29 synapse had the same striking effect on the tonic component of LFS firing as did the removal of L30 itself, with little effect on the maximum frequency of the phasic response. Removing lateral inhibition by taking out the L30-L34 synapse had no effect on motor neuron firing. This was presumably due to the minimal role L34 plays in the network. These results indicate that recurrent inhibition plays a much more important role than lateral inhibition in this circuit. Removal of the electrical coupling between the L29 and L30 neurons had no effect on either the phasic or tonic LFS firing components. To assess whether the negligible effect of removing electrical coupling was due to our use of just a single-model L29 and L30, we constructed an additional simulation with five L29s coupled to three L30s. We found that removing this electrical coupling still had a negligible effect on LFS firing responses to sensory input (not shown). The functional role of the electrical coupling between these neurons thus remains undetermined.

DISCUSSION

Construction of the model network

In this study we constructed a realistic model of one component of the *Aplysia* siphon-elicited siphon-withdrawal reflex circuit, consisting of the LFS motor neurons and all 10 interneurons (5 L29s, 3 L30s, 2 L34s) known to convey excitatory input to them. Although the full circuit contains three other central siphon motor neuron groups (e.g., LBS, LDS, RDS), we focused on the LFS cells because the number of interneurons processing their input is small enough (Frost and Kandel 1995) to make a complete realistic computer simulation of known cells and synapses technically feasible. This particular network also interested us because, although relatively small, it has a number of structural features commonly found in other circuits. These include monosynaptic and polysynaptic sensory neuron to motor neuron pathways, excitatory and inhibitory interneurons, chemical and electrical synapses, and a layer of interneuronal processing that includes both recurrent and lateral inhibition. We were thus motivated by the desire to characterize, within a single circuit, the detailed functional roles of a number of ''building blocks'' (Getting 1989b) that are common elements of most nervous systems.

To do this, we began by individually modeling each of the four cell types and 10 synaptic connections in the circuit on the basis of our own physiological measurements of each component. A key feature of our approach was that the model network replicated the typical, or median, cell or synapse of each type, rather than a single arbitrarily selected example. In this way we avoided modeling just our ''favorite'' or strongest examples—data selection that could have biased network performance (see Koch and Bower 1992 for a discussion of this point). Furthermore, after we constructed each model neuron and synapse, we made no further changes to their free parameters—again, to avoid biasing model performance toward a desired outcome.

Although we took great care to construct model neurons that displayed realistic firing behavior, we made no attempt to match the waveforms of the spike undershoots themselves, which arise from voltage- and calcium-dependent potassium conductances that we did not directly characterize. Integrate-and-fire model cells such as ours are thus phenomenological in nature (see Segev 1992 for a discussion of different modeling schemes); nonetheless, we were able to construct model cells that responded very much like the corresponding real neurons over a large range of injected currents.

Model synapses were constructed to have the same PSP waveforms as their biological counterparts. However, rather than set each model PSP to have the same absolute amplitude as its real counterpart, we instead adjusted it to have the same effect on postsynaptic firing (excitatory or inhibitory) as the median strength example from our data set for that synapse. This procedure, also used by Getting (1989a), ensured that each synaptic connection had the same functional strength as its typical biological counterpart. Another useful feature of this method was that it also roughly incorporated changes in synaptic strength that occur during normal firing

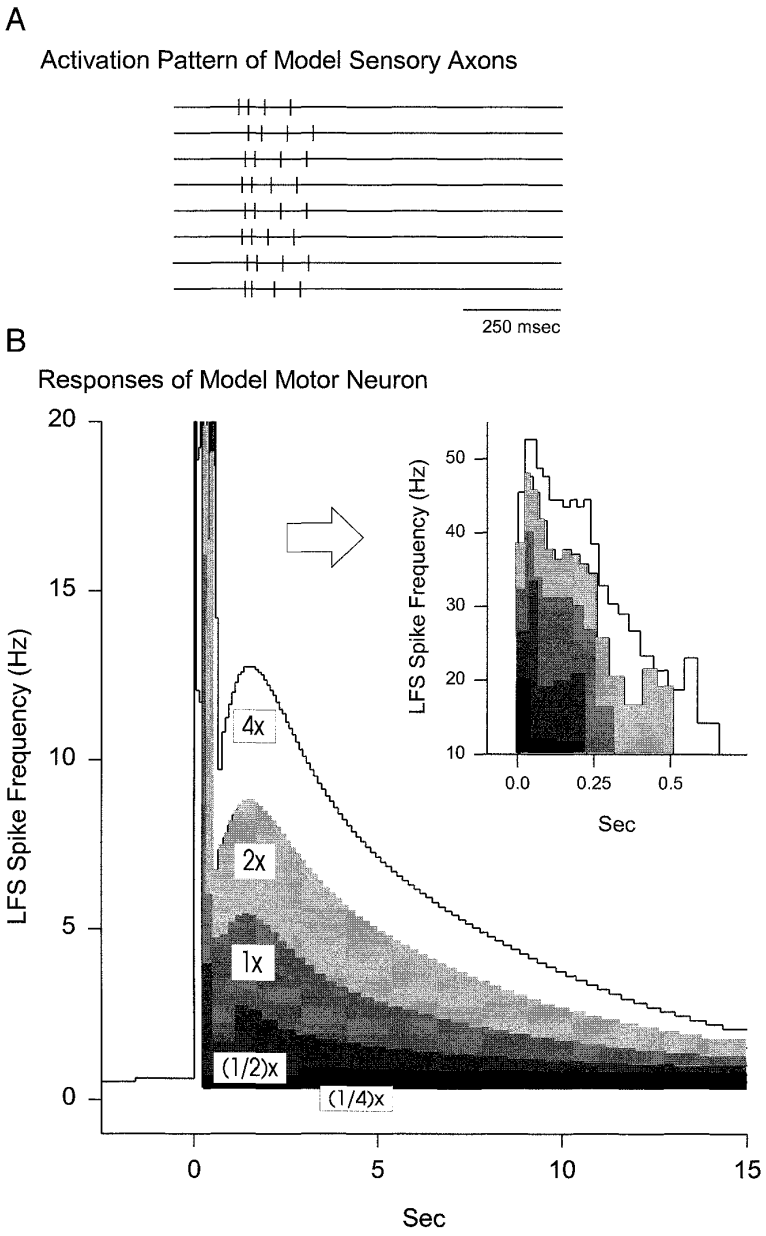

FIG. 12. Responses of the control model network to different intensities of sensory input. *A*: activation pattern of model sensory axons used throughout the study. This sensory train had a population frequency profile similar to that displayed by the LE siphon sensory neurons in response to 4-g tactile siphon stimuli (see RESULTS). *B*: model LFS response, expressed as instantaneous frequency vs. time from stimulus onset, to a range of sensory input intensities. Sensory input strength to the network was varied by keeping the sensory axon activation pattern constant and multiplying the synaptic weight (W) of all sensory neuron synaptic conductances in the network by a constant ratio (1/4, 1/2, 1, 2, and 4). The response of the control model network is the $1 \times W$ response. *Inset*: expanded view of the phasic component of the response.

activity, such as homosynaptic depression at the LE sensory neuron synapses (Castellucci and Kandel 1976) and homosynaptic facilitation at the L30 inhibitory synapses (Fischer and Carew 1993). For example, setting the strength of the model L30 IPSP to match the amplitude of the unfacilitated real IPSP elicited by a single L30 action potential would have led us to underrepresent its actual inhibitory effectiveness during normal firing trains by severalfold.

Two known elements of the LFS component of the siphon-elicited siphon-withdrawal circuit were not included in the model network. Inhibitory cell L16 (Frost and Kandel 1995; Hawkins et al. 1981) was omitted because recent work has shown that this neuron does not reliably inhibit LFS excitatory input elicited by siphon stimulation (Wright and Carew 1995). The L29 interneurons, which make strong conventional EPSPs onto the LFS cells, also produce presynaptic facilitation of the LE neurons (Hawkins and Schacher 1989; Hawkins et al. 1981). We chose not to include this modulation in the model network because it seemed unlikely that the L29s produce significant modulation of LE output during the brief sensory neuron burst associated with a single elicitation of the reflex.

Optical recording studies (Tsau et al. 1994) have shown that siphon stimulation activates neurons in the pleural and pedal ganglia as well as the abdominal ganglion, raising the issue of whether, had the ring ganglia been included in our preparations, we might have obtained substantially different LFS responses to siphon stimulation. Two observations suggest that this is not the case. First, Hickie (1994) reported similar LFS responses to tactile siphon stimulation when the ring ganglia were included in the preparation. Second, in our own experiments in which the ring ganglia were left attached, we found that a range of punctate siphon stimuli (1, 4, and 14 g) elicited the same stereotypic phasic/tonic LFS firing response observed in our normal isolated abdominal ganglion preparation.

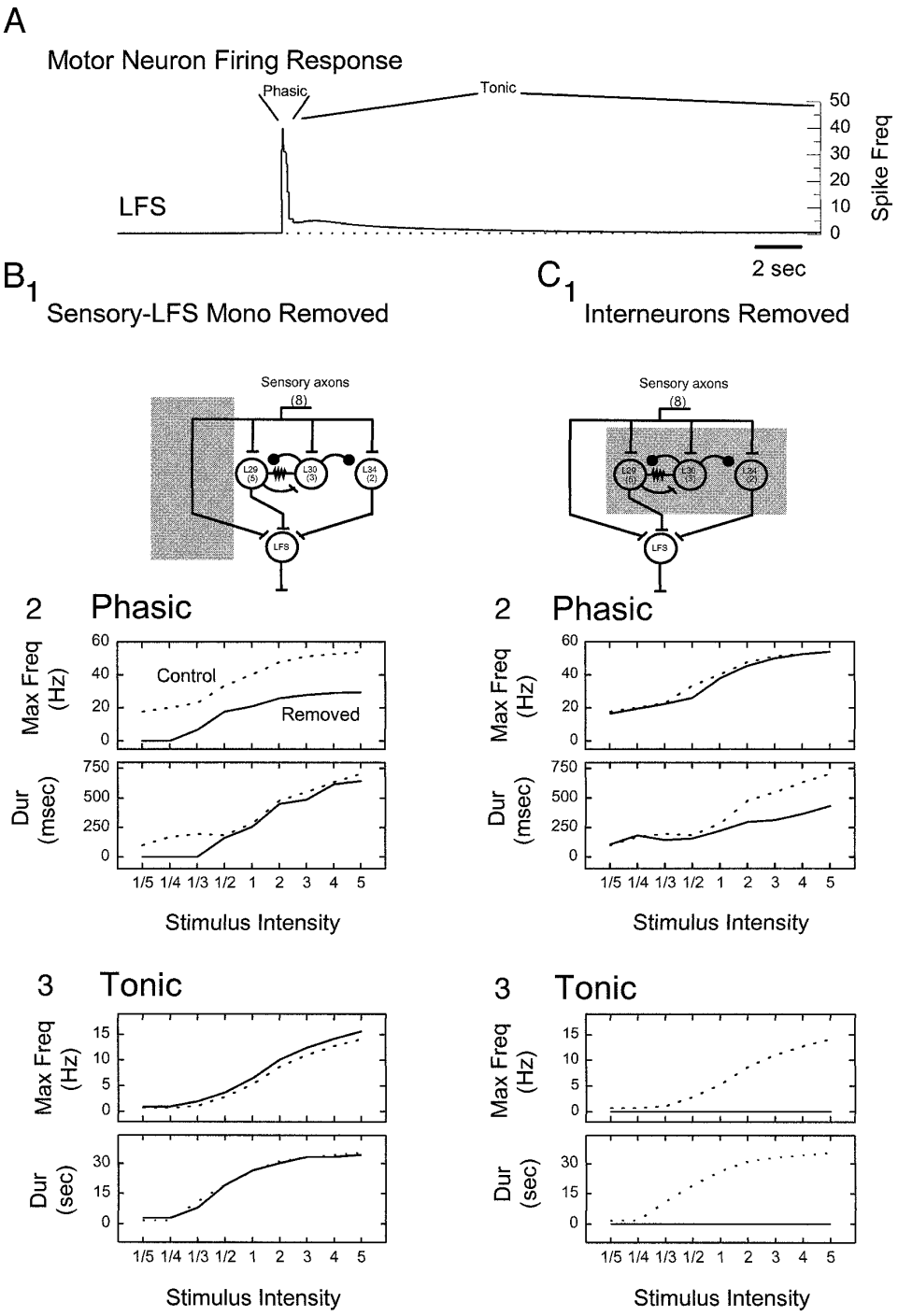

FIG. 13. Roles of the monosynaptic vs. polysynaptic pathways. *A*: instantaneous frequency of model LFS response to input strength of x1 (see Figs. 11*B* and 12*B*). In all graphs the dotted line represents the response of the unmodified model network (control), and the solid line represents the response of the control network with the indicated circuit element subtracted out (removed). Tonic response duration was measured as the time taken for the firing response to decay to 1 Hz. *B1*: diagram indicating removal of the monosynaptic pathway (shaded area). *B2*: removal of the monosynaptic pathway resulted in a decreased maximal phasic response frequency at all input intensities (*top graph*) and a decreased duration of the phasic response at low intensities only (*bottom graph*). *B3*: removal of the monosynaptic pathway had a negligible effect on either component of the tonic firing response. *C1*: diagram indicating removal of the polysynaptic pathway (shaded area). *C2*: removal of the polysynaptic pathway resulted in little or no decrease in the maximum frequency of the phasic response at all input intensities (*top graph*), and a decreased phasic response duration at moderate to high input intensities (*bottom graph*). *C3*: removal of the polysynaptic pathway eliminated both components of the tonic LFS response at all stimulus intensities.

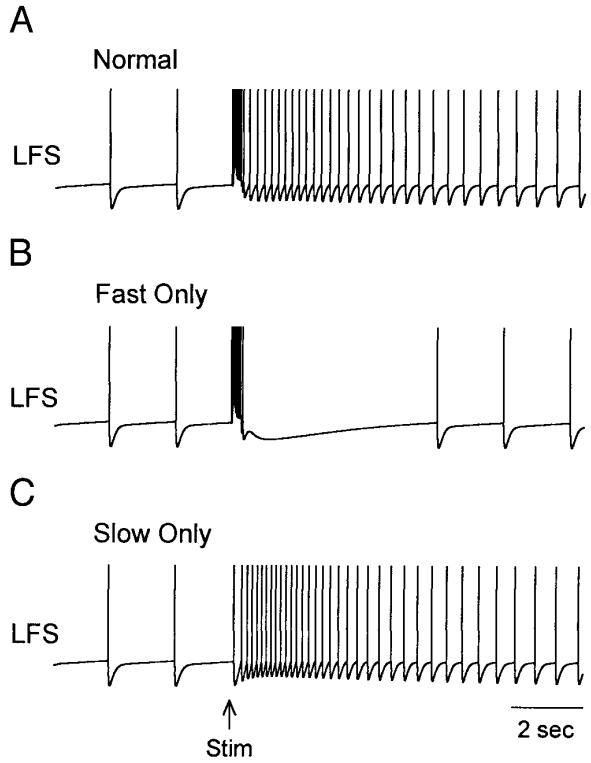

FIG. 14. Tonic LFS firing response is entirely mediated by the slow components of the interneuron to LFS connections. *A*: response of the normal model network. *B*: response of the network after deletion of the slow components of the interneuron to LFS fast/slow EPSPs. *C*: response of the network after deletion of all fast synaptic inputs to LFS, leaving only the slow components of the interneuron to LFS connections.

Roles of the different circuit elements

MONOSYNAPTIC PATHWAY CONTRIBUTES ONLY TO THE PHASIC COMPONENT OF THE LFS RESPONSE. Once the model network was constructed, we first used it to address the role of the monosynaptic sensory neuron to motor neuron pathway. This part of the circuit is of special interest because of the large body of work concerning the cellular and molecular mechanisms of learning-related plasticity at the LE-motorneuron synapses (Byrne and Kandel 1996; Hawkins et al. 1993; Kandel and Schwartz 1982). By comparing network behavior in both the presence and absence of the monosynaptic pathway, we determined that this component contributes only to the phasic and not to the tonic portion of the LFS firing response at all stimulus intensities (Fig. 13). On the basis of recent work evaluating the respective contributions of the phasic and tonic components of LFS firing to actual siphon contractions (Frost and Kandel 1995 and unpublished data), it appears that the monosynaptic pathway contributes primarily to the amplitude and not to the overall duration of the reflex contraction. One implication of this is that forms of learning involving changes in reflex duration are likely to involve modifications to the nervous system at sites other than the sensory neuron to motor neuron monosynaptic connection (Lieb and Frost 1992, 1995), such as the sensory neuron to interneuron connections (Frost and Kandel 1995) and other circuit loci (Fischer and Carew 1993, 1995; Frost et al. 1988; Trudeau and Castellucci 1992, 1993a,b).

SLOW EPSPs AT INTERNEURON TO MOTOR NEURON SYNAPSES TRANSFORM BRIEF SENSORY NEURON DISCHARGES INTO LONG-LASTING MOTOR OUTPUT. We next turned to the role of the different interneurons in the LFS firing response. We found that interneuronal recruitment, specifically of L29, was entirely responsible for the tonic component of LFS firing (Fig. 13). This effect was shown to be specifically due to the slow component of the fast/slow L29-LFS EPSP (Fig. 14). These results indicate that L29 is responsible for transforming brief sensory inputs into long-lasting motor neuron firing, which presumably underlies reflex duration. A similar role for recruited excitatory interneurons has been described in physiological (Cleary and Byrne 1993) and modeling studies of the tail withdrawal reflex circuit in *Aplysia* (White et al. 1993).

Neurophysiologists have long taken an interest in how neural circuits generate sustained activity after brief inputs. Two mechanisms suggested to mediate such sustained activity are reverberatory positive feedback loops (Deadwyler et al. 1988; Gillette et al. 1978; Lorente de No 1938; Roberts et al. 1984; Stringer and Lothman 1992) and the activation of long-duration postsynaptic conductances by brief presynaptic firing trains (Brodfuehrer and Friesen 1986; Cleary and Byrne 1993). L29's role corresponds to the latter mechanism.

RECURRENT INHIBITION ACTS TO BRAKE THE FLOW OF EXCITATION IN THE CIRCUIT. Whereas L29 performs as an intensity to duration transformation element in the circuit, we found that the inhibitory interneuron, L30, plays a different role. This neuron, which mediates recurrent inhibition of L29 and lateral inhibition of L34, has a braking function in the circuit, acting to suppress the flow of excitatory information to the LFS cells (Fig. 15). Recurrent inhibition has long been hypothesized to play a similar control function in vertebrate circuits (Eccles 1964; Hultborn et al. 1979; Pompieno 1984; Renshaw 1941; Shoemaker and Hannaford 1994), and such a braking role for L30 was previously suggested on the basis of both physiological (Fischer and Carew 1993, 1995; Frost and Kandel 1995; Frost et al. 1988; Trudeau and Castellucci 1993a,b) as well as modeling studies of this circuit (Blazis et al. 1993; Fisher et al. 1995). One important function of this built-in inhibition in the siphon-withdrawal circuit may be to serve as a variable gain control element (Frost 1987), because the L30 synapses are strengthened in some circumstances (Fischer and Carew 1993, 1995) and weakened in others (Frost et al. 1988; Trudeau and Castellucci 1993a,b).

CONTRIBUTIONS MADE BY SOME CIRCUIT ELEMENTS VARY WITH STIMULUS INTENSITY. The modeling results discussed so far could be classified as objective confirmations of insights and predictions derived from physiological studies. Although such hypothesis testing is a powerful and worthwhile use of realistic network modeling, some of our most intriguing results were those we had not directly anticipated before beginning this project. Several of these results concerned the finding that some circuit elements contribute differently to LFS firing with increasing stimulus intensity (Figs. 13 and 15).

For example, whereas the monosynaptic pathway contributed to the maximum frequency of the phasic LFS response at all intensities, it contributed to its duration only at low intensities. Among the interneurons, L29 was found to con-

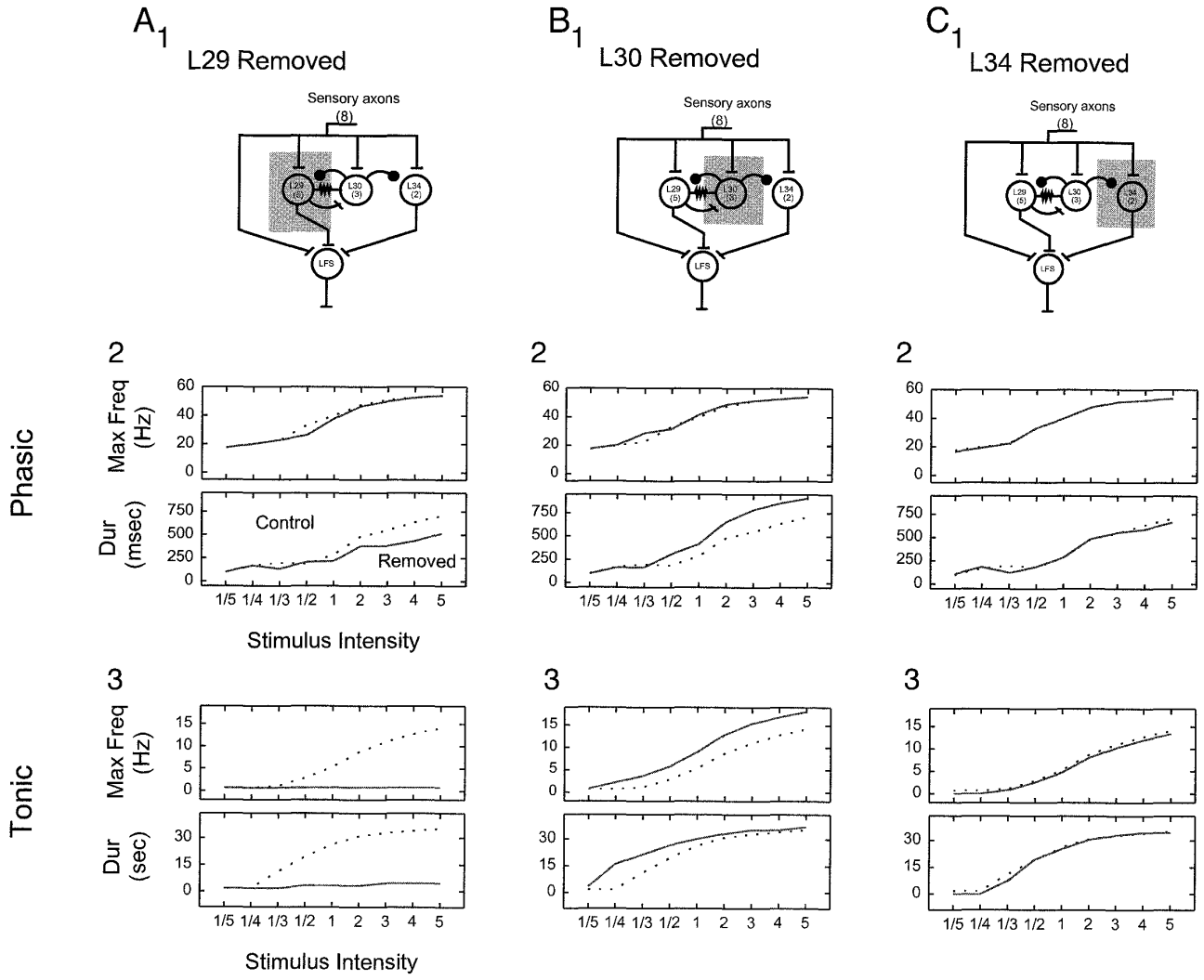

FIG. 15. Roles of the different circuit interneurons. *A1*: diagram indicating removal of L29 from the model circuit (shaded area). *A2*: removal of L29 had no effect on the maximal frequency of the phasic response (*top graph*), but decreased its duration at the higher stimulus intensities (*bottom graph*). In all graphs the dotted line represents the response of the control model network, and the solid line represents the response of the modified network. *A3*: removal of L29 virtually abolished both aspects of the tonic response. *B1*: diagram indicating removal of L30 (shaded area). *B2*: removal of L30 had no effect on the maximal frequency of the phasic response (*top graph*), but did increase its duration (*bottom graph*). *B3*: removal of L30 increased both components of the tonic response, with the effect on response duration being greatest at the lower stimulus intensities. *C1*: diagram indicating removal of L34 (shaded area). *C2*: removal of L34 had no effect on either component of the phasic LFS response. *C3*: removal of L34 had no effect on either component of the tonic LFS response.

tribute most importantly to the duration of the tonic LFS firing response at moderate to high stimulus intensities (Fig. 15). L30, on the other hand, contributed most importantly at the lowest intensities (Fig. 15).

Our efforts to understand the basis of L30's intensity-dependent contribution to LFS tonic firing led us to do some exploratory simulations with the use of model L30s constructed with explicitly different current-frequency relationships (Fig. 16). From this we concluded that L30's asymptotic current-frequency relationship (Fig. 4*A*) was responsible for its intensity-dependent effect on the duration of LFS tonic firing. Because of the sensitivity of this effect, further work would be useful to more accurately describe the shape of the real L30 current-frequency relationship. Intensity-dependent contributions by different circuit elements have implications for the functional significance of learning-related plasticity stored at various sites in the network (Lieb and Frost 1995).

SOME CIRCUIT ELEMENTS MAKE NO DETECTABLE CONTRIBUTION. Removing some circuit components had virtually no effect on LFS firing. These included the excitatory interneuron L34, the L29-L30 electrical connection, and the L30-L34 lateral inhibitory connection. The assignment of a minor role for L34 (and thus inhibition of L34) is not simply due to the fact that we evaluated it by subtracting rather than adding it to the network: L34 still made a negligible contribution to the duration of tonic LFS firing when it was the only excitatory interneuron present (Fig. 15*A3*). Its minor role in this network was due to its weak functional connection onto LFS (Fig. 9).

These results do not, however, allow us to conclude that L34 is a neuron without function. For example, its contribution to LFS firing may be stronger in response to stimulation of other body sites; previous work has shown that the L29s are not activated by head stimuli (Hawkins and Schacher 1989),

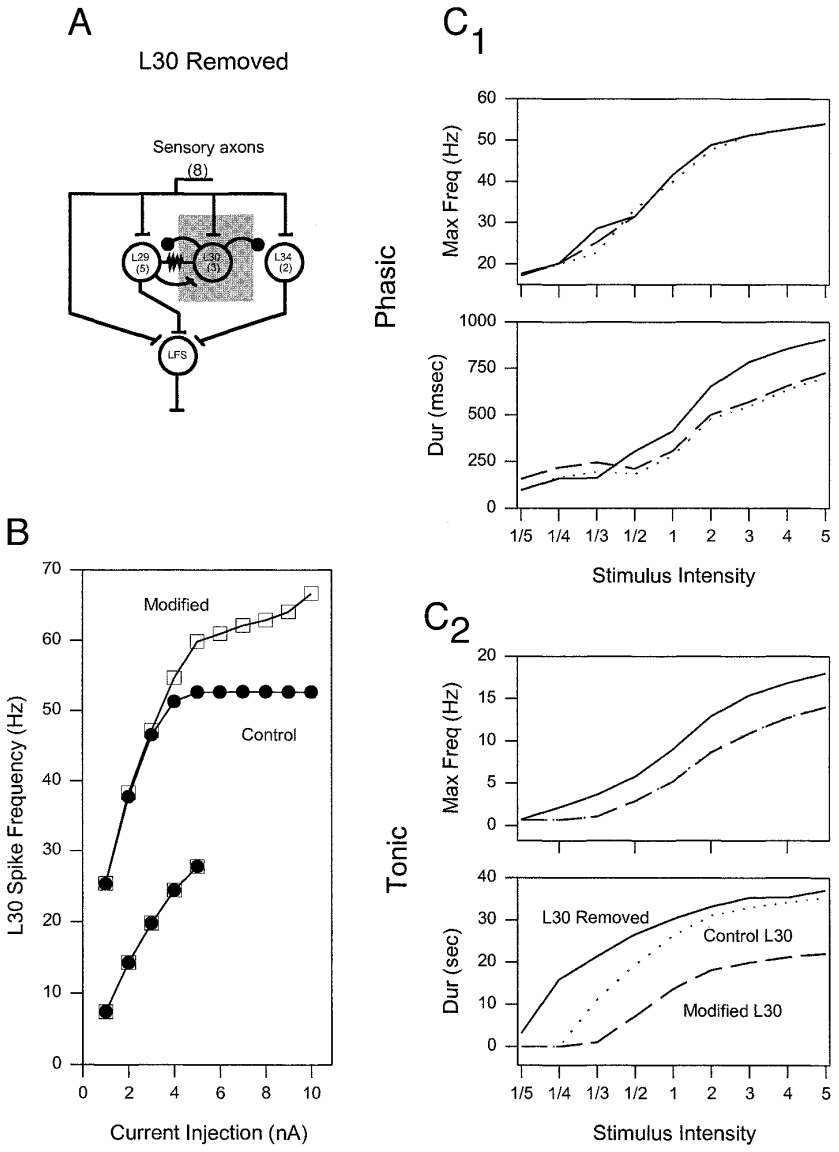

FIG. 16. Shape of the L30 current-frequency curve is responsible for L30's inability to influence the duration of tonic LFS firing at high stimulus intensities. *A*: diagram indicating removal of L30. *B*: comparison of current-frequency plots for the model L30 used in our study (control) and a modified model L30 containing shunt conductances identical to those used in the model L34. The current-frequency plot of the modified L30 lacks the asymptotic shape of the control L30. *C1*: there was no significant difference in the effect of either L30 on the phasic component of the LFS firing response to a wide range of stimulus intensities. Dotted line: LFS response with the control L30 in the model network. Dashed line: LFS response with the modified L30 in the model network. Solid line: LFS response with L30 removed from the model network. *C2*: modified L30 inhibited the duration of the tonic LFS response at all stimulus intensities, indicating the importance of the asymptotic shape of the control L30 current-frequency plot in conferring L30's intensity-dependent influence over this component of LFS firing.

suggesting that other circuit elements mediate siphon contractions to head stimuli. L34 may also make more powerful synaptic connections onto other motor neurons. It also remains possible that its role in the LFS network is subject to modulatory control.

Testable predictions of the model network

One advantage of modeling small circuits of neurons is that the simulations can be used interactively with tractable physiological experiments to independently assess the results of the other. For instance, although the network was constructed on the basis of neuronal responses to a single stimulus intensity, we can test its validity by assessing whether the real network responds similarly to a wide range of input intensities (an initial such comparison was described in the RESULTS, in the section on the robustness of the model network). Our results lead to several other predictions that can be tested with future experimental work. First, the removal of all five L29s from the circuit (such as by hyperpolarization or cell ablation) should significantly reduce the tonic LFS firing response and yet have little effect on the maximum frequency of the phasic response (Fig. 15*A*). Second, removal of all three L30s should increase the duration of LFS tonic firing, but only in response to low- to moderate-strength siphon stimuli (Fig. 15*B*). Third, removal of the two L34s should have virtually no effect on any component of the LFS response to siphon stimulation. Physiological studies have already shown that removing a single L29 (Fischer and Carew 1993) or two L30s (Fischer and Carew 1995) can change the amplitude of the phasic LFS input to weak siphon stimulation, but it is not yet known to what degree such manipulations affect the phasic or tonic LFS firing response. Finally, all of the results concerning intensity-dependent contributions of the different circuit elements are, in principle, testable through similar physiological subtraction experiments.

Conclusion

This study represents a detailed dissection of the functional roles of the different elements of the siphon-elicited

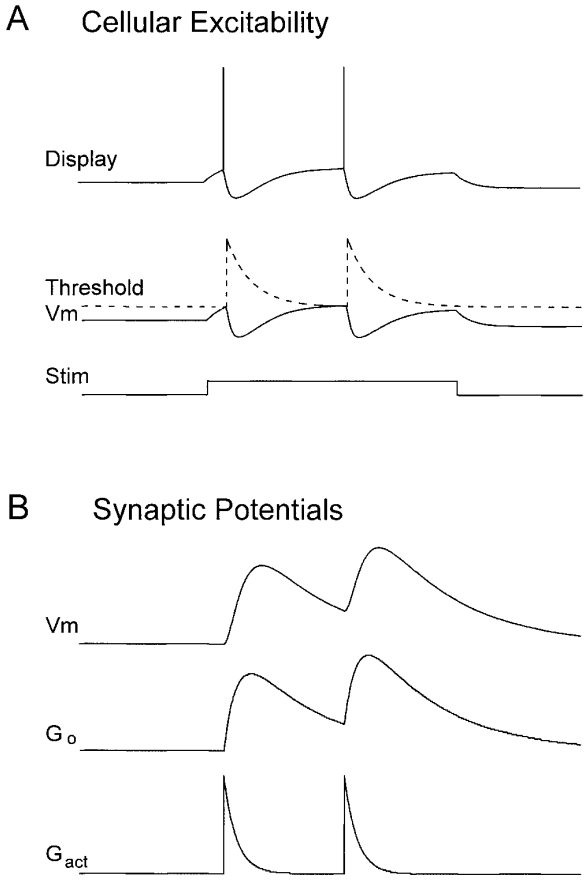

FIG. 17. Simulation of cellular excitability and synaptic potentials. *A*: integrate-and-fire scheme for modeling cellular excitability. The simulation tracks 2 separate variables, membrane potential (Vm) and threshold. Whenever the 2 meet, such as in response to depolarizing current injection (Stim), an action potential is noted, threshold is reset to a specified value from which it decays with a specified time constant, and spike undershoot conductances are activated. *B*: computation of synaptic potentials. Each action potential in the presynaptic neuron causes the instantaneous creation of a population of activated but not yet open postsynaptic conductance channels (G_{act}). As these channels open, G_{act} decreases with a specified time constant, and the population of open channels (G_o) builds. This population in turn decays with a 2nd specified time constant. G_o represents the time-dependent synaptic conductance that underlies the synaptic potential (Vm).

siphon-withdrawal circuit in *Aplysia* (see also Blazis et al. 1993). Because several sites in this network are known to store learning-related information (Frost et al. 1988; Trudeau and Castellucci 1993b), these results are relevant not just to understanding the basic functional dynamics of the circuit but also for elucidating the functional significance of the distributed storage of learned information in *Aplysia* (Lieb and Frost 1992, 1995). Furthermore, because many vertebrate and invertebrate circuits perform similar tasks, and contain similar information processing elements (Dowling 1992), many of our results may be expected to have general relevance.

APPENDIX

Description of equations

GENERAL FEATURES. Simulations were performed with MARIO, a network modeling program originally created by Getting and Lawrence (Getting 1989a) and since developed further by Frost and Lawrence. All neurons were modeled with an integrate-and-fire simulation scheme (Fig. 17*A*). In this approach, action potential waveforms are not calculated. Instead, action potentials are treated simply as instantaneous events that occur whenever membrane potential meets a separately calculated threshold variable. When such a meeting occurs, an action potential is noted by the program, synaptic conductances are activated in all postsynaptic targets of the cell, time-dependent conductances giving rise to an action potential undershoot are activated, and the threshold variable is instantaneously reset to a positive potential, from which it exponentially decays back to its steady-state level. By adjusting the free parameters controlling threshold and spike undershoot, one can produce model neurons that fire in very similar fashion to their biological counterparts, i.e., with comparable firing frequencies and spike frequency adaptation to a wide range of input currents.

Integrate-and-fire model neurons are phenomenological in nature: each model cell mimics the unique firing frequencies and spike frequency adaptation properties of its counterpart neuron in the nervous system. No attempt is made to duplicate the actual set of voltage- and time-dependent membrane conductances underlying these responses in the real neurons, as in many Hodgkin-Huxley style approaches. Integrate-and-fire approaches are well suited for studying the roles played by specific neurons and synapses in network function. They are not useful, however, for investigating biophysical mechanisms underlying cellular features like the action potential or neurotransmitter release.

The equations used in our simulations are as follows.

THRESHOLD. In our particular integrate-and-fire scheme, threshold potential was an explicitly defined function. An action potential caused threshold to be instantaneously reset from its resting level to a more depolarized reset potential, from which it exponentially decayed with a specified time constant (Fig. 17*A;* Getting 1989a; Perkel et al. 1981). Threshold was defined as

$$\theta(t) = \theta_{ss} + (\theta_r - \theta_{ss})e^{(t_x - t)/\theta_\tau} \quad (1)$$

where θ_{ss} is steady-state threshold (measured), θ_r is threshold reset potential (free parameter), θ_τ is the time constant of decay of threshold (free parameter), t_x is the time of previous action potential since start of simulation, and t is the time since start of simulation. See text for the procedures used to obtain all measured parameters and to set all free parameters in the simulation.

MEMBRANE POTENTIAL. Membrane potential was calculated using a fourth-order Runge Kutta numerical integration, as the sum of all membrane currents divided by the measured input capacitance of the neuron

$$\frac{dV}{dt} = -\frac{1}{C}\left(I_{leak} + \Sigma I_{syn} + \Sigma I_{undershoot} + \Sigma I_{coupl} + \Sigma I_{shunt} - I_{stim}\right) \quad (2)$$

where V is membrane potential, t is time, C is input capacitance, I_{leak} is leakage current, ΣI_{syn} is chemical synaptic current, $\Sigma I_{undershoot}$ is spike undershoot current, ΣI_{coupl} is electrical synaptic current, ΣI_{shunt} is voltage-dependent shunt current, and I_{stim} is stimulus current. The separate terms of this equation were computed each time step as follows.

LEAKAGE CURRENT. Leakage current, the current that flowed through the fixed R_{input} of each neuron whenever its membrane potential differed from V_r, was calculated as

$$I_{leak} = \frac{V - V_r}{R_{input}} \quad (3)$$

where V is membrane potential (calculated), V_r is resting potential (measured), and R_{input} is input resistance (measured).

CHEMICAL SYNAPTIC CURRENTS. Chemical synapses were modeled as an increased conductance, first-order kinetic process (see Perkel et al. 1981), in which each presynaptic action potential activated a variable membrane conductance that opened and closed

with separately specifiable rate constants. The conceptual scheme for this was

$$\text{Presynaptic action potential} \Rightarrow G_{act} \overset{open}{\rightarrow} G_o \overset{close}{\rightarrow} \text{Closed state} \quad (4)$$

where G_{act} is the activated but closed conductance state and G_o is the open conductance state. Synaptic conductance was computed by integrating a pair of coupled differential equations that together described the rate of change of G_o with time (see also Perkel et al. 1981)

$$\frac{dG_{act}}{dt} = -\frac{G_{act}}{\tau_{open}} \quad (5)$$

$$\frac{dG_o}{dt} = \frac{G_{act}}{\tau_{open}} - \frac{G_o}{\tau_{close}} \quad (6)$$

where τ_{open} and τ_{close} are the opening and closing time constants (free parameters), respectively, for the open conductance state G_o. At the onset of each simulation, G_{act} for each synapse was 0. After each presynaptic action potential, G_{act} was incremented by 1 from its current value, from which it exponentially decayed toward 0 with a time constant of τ_{open} (Fig. 17*B*). The numerical integration of dG_o/dt during each time step of the simulation provided the current value of G_o needed to calculate the synaptic current

$$I_{syn} = W \cdot G_o \cdot (V - E_{rev}) \cdot A \quad (7)$$

where W is synaptic weight (free parameter), G_o is synaptic conductance, V is membrane potential, E_{rev} is reversal potential for synaptic conductance (−60 mV for IPSPs, +10 mV for EPSPs), and A is an empirically derived normalization term that was introduced to minimize changes in synaptic potential amplitude when adjusting τ_{open} and τ_{close} during construction of model synapses. The normalization term, a constant, was calculated as

$$A = \frac{1}{(4e^{(-3.15/(\tau_{close}/\tau_{open}))}) + 1} \quad (8)$$

At each time step, all active synaptic currents were summed for each postsynaptic neuron to yield the ΣI_{syn} term used in *Eq. 2*. A comparison of the waveforms of G_{act}, G_o, and V for a typical fast EPSP is shown in Fig. 17*B*.

ACTION POTENTIAL UNDERSHOOT CURRENTS. Although action potential waveforms were not computed in our integrate-and-fire simulation scheme, action potential undershoots were. As in biological neurons, spike undershoots served to control the firing frequency and adaptation properties of the model neurons. Thus, for each model neuron, whenever membrane potential reached threshold an action potential was noted by the program and a pair of spike undershoot conductances were activated. These were treated computationally as recurrent inhibitory synaptic connections with E_{rev}s of −80 mV

$$I_{undershoot} = W \cdot G_o \cdot (V - E_{rev}) \cdot A \quad (9)$$

ELECTRICAL SYNAPTIC CURRENTS. Electrical coupling was implemented by introducing unidirectional resistances between the coupled neurons. This method allowed for asymmetrical coupling, if such was observed experimentally. The electrical synaptic current flowing from cell A to cell B was computed as

$$I_{coupl} = \frac{V_A - V_B}{R_{coupl}} \quad (10)$$

where V_A is membrane potential of cell A, V_B is membrane potential of cell B, and R_{coupl} is coupling resistance of electrical synapse in the direction from cell A to cell B.

VOLTAGE-DEPENDENT SHUNT CURRENTS. We also added voltage-dependent shunt conductances to all neurons, with E_{rev}s equal to the V_r. These conductances were adjusted to cause the firing rate of the model neuron to level off at the highest levels of injected currents, as the biological neurons did. This conductance was computed as

$$\Sigma I_{shunt} = G \cdot m \cdot h \cdot (V - E_{rev}) \quad (11)$$

where m and h represent the activation and inactivation variables for the conductance, respectively. In all of our model neurons, h was set equal to 1 (i.e., the shunt conductances were noninactivating). During the simulation, m was calculated as

$$\frac{dm}{dt} = \frac{(m_\infty - m)}{\tau_m} \quad (12)$$

where m_∞ is steady-state activation and τ_m is time constant of activation. Steady-state activation, in turn, was calculated as

$$m_\infty = \frac{1}{1 + e^{(V_m + B)/C}} \quad (13)$$

where B represents the membrane potential at which the steady-state activation was half-maximal, and C represents the slope parameter of the activation curve of the conductance. Of the above, G, τ_m, B, and C were free parameters, E_{rev} was set to V_r, and m, m_∞, h, and V were variables calculated by the program.

STIMULUS CURRENT. Stimulus currents were injected into model neurons in the form of positive or negative constant current pulses.

The authors thank Dr. P. S. Katz for useful discussions during this work. We also thank Drs. P. S. Katz and L. Eliot for comments on earlier versions of the manuscript, L. Wu for assisting with some of the data collection, and D. Lawrence for programming enhancements to MARIO.

This work was supported by National Institute of Mental Health Grants MH-10471 to J. R. Lieb, Jr. and MH-48536 to W. N. Frost.

Address for reprint requests: W. N. Frost, P.O. Box 20708, Dept. of Neurobiology and Anatomy, University of Texas, Houston Health Science Center, Houston, TX 77225.

Received 13 May 1996; accepted in final form 1 November 1996.

REFERENCES

BLAZIS, D.E.J., FISCHER, T. M., AND CAREW, T. J. A neural network model of inhibitory information processing in *Aplysia. Neural Comput.* 5: 213–227, 1993.

BRODFUEHRER, P. D. AND FRIESEN, W. O. Initiation of swimming activity by trigger neurons in the leech subesophageal ganglion. II. Role of segmental swim-initiating interneurons. *J. Comp. Physiol. A Sens. Neural Behav. Physiol.* 159: 503–510, 1986.

BYRNE, J. H. Analysis of synaptic depression contributing to habituation of gill withdrawal reflex in *Aplysia californica. J. Neurophysiol.* 48: 431–438, 1982.

BYRNE, J. H., CASTELLUCCI, V. F., CAREW, T. J., AND KANDEL, E. R. Stimulus-response relations and stability of mechanoreceptor and motor neurons mediating defensive gill-withdrawal reflex in *Aplysia. J. Neurophysiol.* 41: 402–417, 1978a.

BYRNE, J. H., CASTELLUCCI, V. F., AND KANDEL, E. R. Receptive fields and response properties of mechanoreceptor neurons innervating siphon skin and mantle shelf in *Aplysia. J. Neurophysiol.* 37: 1041–1064, 1974.

BYRNE, J. H., CASTELLUCCI, V. F., AND KANDEL, E. R. Contribution of individual mechanoreceptor sensory neurons to defensive gill-withdrawal reflex in *Aplysia. J. Neurophysiol.* 41: 418–431, 1978b.

BYRNE, J. H. AND KANDEL, E. R. Presynaptic facilitation revisited: state and time dependence. *J. Neurosci.* 16: 425–435, 1996.

CASTELLUCCI, V. AND KANDEL, E. R. Presynaptic facilitation as a mechanism for behavioral sensitization in *Aplysia. Science Wash. DC* 194: 1176–1178, 1976.

CASTELLUCCI, V., PINSKER, H., KUPFERMANN, I., AND KANDEL, E. R. Neuronal mechanisms of habituation and dishabituation of the gill-withdrawal reflex in *Aplysia. Science Wash. DC* 167: 1745–1748, 1970.

CLEARY, L. J. AND BYRNE, J. H. Identification and characterization of a multifunction neuron contributing to defensive arousal in *Aplysia. J. Neurophysiol.* 70: 1767–1776, 1993.

CLEARY, L. J., BYRNE, J. H., AND FROST, W. N. Role of interneurons in defensive withdrawal reflexes in *Aplysia. Learn. Memory* 2: 133–151, 1995.

COHEN, T. E., HENZI, V., KANDEL, E. R., AND HAWKINS, R. D. Further behavioral and cellular studies of dishabituation and sensitization in *Aplysia*. *Soc. Neurosci. Abstr.* 17: 1302, 1991.

DEADWYLER, S. A., HAMPSON, R. E., FOSTER, T. E., AND MARLOW, G. The functional significance of long-term potentiation: relation to sensory processing by hippocampal circuits. In: *Long-Term Potentiation: From Biophysics to Behavior*, edited by P. W. Landfield and S. A. Deadwyler. New York: Liss, 1988, p. 499–534.

DOWLING, J. E. *Neurons and Networks.* Cambridge, MA: Harvard Univ. Press, 1992.

DUBUC, B. AND CASTELLUCCI, V. Receptive fields and properties of a new cluster of mechanoreceptor neurons innervating the mantle region and the branchial cavity of the marine mollusk *Aplysia californica*. *J. Exp. Biol.* 156: 315–334, 1991.

ECCLES, J. C. *The Physiology of Synapses.* Berlin: Springer-Verlag, 1964.

FISCHER, T. M. AND CAREW, T. J. Activity-dependent potentiation of recurrent inhibition: a mechanism for dynamic gain control in the siphon-withdrawal reflex of *Aplysia*. *J. Neurosci.* 13: 1302–1314, 1993.

FISCHER, T. M. AND CAREW, T. J. Cutaneous activation of the inhibitory L30 interneurons provides a mechanism for regulating adaptive gain control in the siphon-withdrawal reflex of *Aplysia*. *J. Neurosci.* 15: 762–773, 1995.

FISHER, S. A., FISCHER, T. M., AND CAREW, T. J. A computational model of activity-dependent potentiation and its external modulation at L30 inhibitory synapses in *Aplysia*. *Soc. Neurosci. Abstr.* 21: 1457, 1995.

FROST, W. N. *Mechanisms Contributing to Short- and Long-Term Sensitization in Aplysia* (PhD dissertation). New York: Columbia Univ., 1987.

FROST, W. N., CLARK, G. A., AND KANDEL, E. R. Parallel processing of short-term memory for sensitization in *Aplysia*. *J. Neurobiol.* 19: 297–334, 1988.

FROST, W. N. AND KANDEL, E. R. Structure of the network mediating siphon-elicited siphon-withdrawal in *Aplysia*. *J. Neurophysiol.* 73: 2413–2427, 1995.

FROST, W. N., WU, L. G., AND LIEB, J. Simulation of the *Aplysia* siphon-withdrawal reflex circuit: slow components of interneuronal synapses contribute to the mediation of reflex duration. *Soc. Neurosci. Abstr.* 17: 1390, 1991.

GETTING, P. A. Mechanisms of pattern generation underlying swimming in *Tritonia*. II. Network reconstruction. *J. Neurophysiol.* 49: 1017–1035, 1983.

GETTING, P. A. Reconstruction of small neural networks. In: *Methods in Neuronal Modeling: From Synapses to Networks*, edited by C. Koch and I. Segev. Cambridge, MA: MIT Press, 1989a.

GETTING, P. A. Emerging principles governing the operation of neural networks. *Annu. Rev. Neurosci.* 12: 185–204, 1989b.

GILLETTE, R., KOVAC, M. P., AND DAVIS, W. J. Command neurons in *Pleurobranchaea* receive synaptic feedback from the motor network they excite. *Science Wash. DC* 199: 798–801, 1978.

HAWKINS, R. D., CASTELLUCCI, V. F., AND KANDEL, E. R. Interneurons involved in mediation and modulation of gill-withdrawal reflex in *Aplysia*. I. Identification and characterization. *J. Neurophysiol.* 45: 304–314, 1981.

HAWKINS, R. D., KANDEL, E. R., AND SIEGELBAUM, S. A. Learning to modulate transmitter release: themes and variations in synaptic plasticity. *Annu. Rev. Neurosci.* 16: 625–665, 1993.

HAWKINS, R. D. AND SCHACHER, S. Identified facilitator neurons L29 and L28 are excited by cutaneous stimuli used in dishabituation, sensitization, and classical conditioning of *Aplysia*. *J. Neurosci.* 9: 4236–4245, 1989.

HICKIE, C. *Functional and Motor Neuronal Analysis of Defensive Siphon Responses in Aplysia californica* (PhD dissertation). Houston, TX: Univ. of Texas at Houston Health Science Center, 1994.

HICKIE, C. AND WALTERS, E. T. Motor neuronal control of tail-directed and head-directed siphon responses in *Aplysia californica*. *J. Neurophysiol.* 74: 307–321, 1995.

HULTBORN, H., LINDSTROM, S., AND WIGSTROM, H. On the function of recurrent inhibition in the spinal cord. *Exp. Brain Res.* 37: 399–403, 1979.

KANDEL, E. R. AND SCHWARTZ, J. H. Molecular biology of learning: modulation of transmitter release. *Science Wash. DC* 218: 433–443, 1982.

KANDEL, E. R., SCHWARTZ, J. H., AND JESSEL, T., M. *Principles of Neural Science.* New York: Elsevier, 1991.

KAPLAN, S. W., KANDEL, E. R., AND HAWKINS, R. D. Plasticity in the monosynaptic component of the *Aplysia* gill-withdrawal reflex during habituation, dishabituation, and sensitization. *Soc. Neurosci. Abstr.* 19: 16, 1993.

KOCH, C. AND BOWER, J. M. Experimentalists and modelers: can we all just get along? *Trends Neurosci.* 15: 458–461, 1992.

LIEB, J. R., JR. AND FROST, W. N. Interneuronal plasticity contributes significantly to enhanced motor neuron firing during sensitization of the *Aplysia* siphon-withdrawal reflex. *Soc. Neurosci. Abstr.* 18: 531, 1992.

LIEB, J. R., JR. AND FROST, W. N. Dynamic representation of learned information in a distributed memory in *Aplysia*. *Soc. Neurosci. Abstr.* 21: 1458, 1995.

LORENTE DE NO, R. Analysis of the activity of the chains of internuncial neurons. *J. Neurophysiol.* 1: 207–244, 1938.

PERKEL, D. H., MULLONEY, B., AND BUDELLI, R. W. Quantitative methods for predicting neuronal behavior. *Neuroscience* 6: 823–837, 1981.

POMPEIANO, O. Recurrent inhibition. In: *Handbook of the Spinal Cord*, edited by R. A. Davidoff. New York: Dekker, 1984.

RENSHAW, B. Influence of the discharge of motoneurons upon excitation of neighboring motoneurons. *J. Neurophysiol.* 4: 167–183, 1941.

ROBERTS, A., DALE, N., AND SOFFE, S. R. Sustained responses to brief stimuli: swimming in *Xenopus* embryos. *J. Exp. Biol.* 112: 321–335, 1984.

SEGEV, I. Single neurone models: oversimple, complex, and reduced. *Trends Neurosci.* 15: 414–421, 1992.

SHOEMAKER, M. AND HANNAFORD, B. A study and model of the role of the Renshaw cell in regulating the transient firing rate of the motoneuron. *Biol. Cybern.* 71: 251–262, 1994.

STRINGER, J. L. AND LOTHMAN, E. W. Reverberatory seizure discharges in hippocampal-parahippocampal circuits. *Exp. Neurol.* 116: 198–203, 1992.

TRUDEAU, L. E. AND CASTELLUCCI, V. F. Contribution of polysynaptic pathways in the mediation and plasticity of *Aplysia* gill and siphon-withdrawal reflex: evidence for differential modulation. *J. Neurosci.* 12: 3838–3848, 1992.

TRUDEAU, L. E. AND CASTELLUCCI, V. F. Functional uncoupling of inhibitory interneurons plays an important role in short-term sensitization of the *Aplysia* gill and siphon-withdrawal reflex. *J. Neurosci.* 13: 2126–2135, 1993a.

TRUDEAU, L. E. AND CASTELLUCCI, V. F. Sensitization of the gill and siphon-withdrawal reflex of *Aplysia*: multiple sites of change in the neuronal network. *J. Neurophysiol.* 70: 1210–1220, 1993b.

TSAU, Y., WU, J., HOPP, H., COHEN, L. B., SCHIMINOVICH, D., AND FALK, C. X. Distributed aspects of the response to siphon touch in *Aplysia*: spread of stimulus information and cross-correlation analysis. *J. Neurosci.* 14: 4167–4184, 1994.

WHITE, J. A., ZIV, I., CLEARY, L. J., BAXTER, D. A., AND BYRNE, J. H. The role of interneurons in controlling the tail-withdrawal reflex in *Aplysia*: a network model. *J. Neurophysiol.* 70: 1777–1786, 1993.

WRIGHT, W. G. AND CAREW, T. J. A single identified interneuron gates tail-shock induced inhibition in the siphon-withdrawal reflex of *Aplysia*. *J. Neurosci.* 15: 790–797, 1995.

WRIGHT, W. G., MARCUS E. A., AND CAREW, T. J. A cellular analysis of inhibition in the siphon-withdrawal reflex of *Aplysia*. *J. Neurosci.* 11: 2498–2509, 1991.